Check for updates

Science

RESEARCH ARTICLES

Cite as: H. P. Q. Nguyen *et al.*, *Science*
10.1126/science.aec6413 (2026).

Molecular solar thermal energy storage in Dewar pyrimidone beyond 1.6 MJ/kg

Han P. Q. Nguyen[1,2], Alexander J. Maertens[3], Benjamin A. Baker[1,2], Nathan M.-W. Wu[2], Zihao Ye[3], Qingyang Zhou[3], Qianfeng Qiu[2], Navneet Kaur[2], David B. Berkinsky[2], Katherine E. Shulenberger[2], K. N. Houk[3]*, Grace G. D. Han[1,2]*

[1]Department of Chemistry and Biochemistry, University of California, Santa Barbara, CA, USA. [2]Department of Chemistry, Brandeis University, Waltham, MA, USA. [3]Department of Chemistry and Biochemistry, University of California, Los Angeles, CA, USA.

***Corresponding author. Email: grace_han@ucsb.edu (G.G.D.H.); houk@ucla.edu (K.N.H.)**

Storing sunlight in a compact and rechargeable form remains a central challenge for solar energy utilization. Molecular solar thermal (MOST) energy storage systems, which harness photon energy and release it as heat on demand, provide a direct approach, but have long failed to meet practical benchmarks. Inspired by the architecture of DNA, we report a pyrimidone-based MOST system that stores energy in the strained Dewar photoisomer upon excitation at 300 nm. Designed with sustainability in mind, the system operates solvent-free and remains compatible with aqueous environments while overcoming one of the field's greatest hurdles: the controlled extraction and transfer of stored heat. When catalyzed by acid, the Dewar isomer releases enough heat to boil water (~0.5 mL). These advances help point the way toward decentralized solar heat storage and off-grid energy solutions.

Heating accounts for nearly half of the global energy demand (*1*). Keeping homes warm in winter, providing hot water for daily use, and cooking meals are essential energy services that depend heavily on reliable heat supply. Yet almost two-thirds of this heating energy still comes from fossil fuels such as natural gas, oil, and coal, making heating one of the largest direct sources of carbon emissions (*2*). The transition to a sustainable energy future therefore requires not only carbon-free electricity generation but also clean and storable heat.

Conventional off-grid heating relies on liquid fuels such as heating oil, which can be easily stored and transported while presenting high combustion energy densities (40 MJ kg^{-1}) (*3*). In renewable systems, lithium-ion batteries are widely used for energy storage, with an effective energy density of 0.9 MJ kg^{-1} (*4*). When paired with solar panels, home battery systems can store electricity and power electric heaters, stoves, or boilers via Joule heating, in which electrical energy is directly converted into heat (*5*), enabling renewable thermal energy storage and release.

Recent advances in molecular photoswitches have opened up opportunities across a wide range of fields. These materials can reversibly transform between two or more distinct states under light, enabling applications in soft robotics (*6*), switchable catalysis (*7*), CO_2 capture (*8*), temperature sensing (*9*, *10*), protein modulation (*11*), and mechanically interlocked molecule synthesis (*12*).

Beyond these functions, molecular photoswitches have recently emerged as media for renewable solar energy storage and release, a concept known as molecular solar thermal (MOST) energy storage. In these systems, photon energy is captured and stored in the strained chemical bonds of a metastable photoisomer, which can later be triggered to revert to its thermodynamically stable form, releasing heat. Representative MOST systems include the photoisomerizing azo(hetero)arenes (*13*, *14*), hydrazones (*15*), dihydroazulenes (*16*, *17*), fulvalene diruthenium (*18–20*), norbornadienes (*21–28*), bicyclooctadienes (*29*), azaborinines (*30*, *31*), and curved anthracenes (*32*).

The performance of a MOST compound is determined by several key parameters, which include enhanced light absorption (*33–36*), robust resistance to fatigue (*37–40*), efficient isomerization with high quantum yield (*41–43*), tunable activation energy for reversion to the thermodynamically stable state ($\Delta H^{\ddagger}$) (*44–46*), and large energy storage density ($\Delta H_{storage}$) (*31*, *32*), i.e., energy difference between the stable and metastable states. The latter two properties are particularly crucial, as a sufficiently high $\Delta H^{\ddagger}$ enables long-term energy retention (*47*, *48*), while the historically low $\Delta H_{storage}$ has limited the translation of the MOST concept into practical heating applications (*49*, *50*). To maximize $\Delta H_{storage}$, it is advantageous to focus on small molecules that undergo photoisomerization to highly strained metastable isomers (*51*).

Photoinduced valence isomerization, a pericyclic reaction occurring in some small molecules, has been demonstrated in MOST systems. For instance, norbornadiene undergoes an intramolecular [2+2] photocycloaddition to form quadricyclane, thereby storing energy in a strained cyclic structure (*26*). This system exhibits one of the highest gravimetric energy storage densities of 0.97 MJ kg^{-1} (89 kJ mol^{-1}) among all MOST compounds. Another type of valence isomerization, i.e., Dewar isomerization, which involves photo-induced loss of aromaticity, holds promise for maximizing $\Delta H_{storage}$.

Recently, azaborinines and their Dewar isomers were reported as an emerging MOST system with gravimetric energy densities up to 0.65 MJ kg^{-1} (201 kJ mol^{-1}) per active monomeric unit (*30*, *31*). The notably high molar energy density of this system could be due to the loss of aromaticity upon isomerization, which increases the energy gap between the stable aromatic isomer and metastable non-aromatic isomer (*52*–*54*).

However, the absorption of norbornadienes is restricted to the UV-C range (< 280 nm), requiring artificial light sources (*55*) for energy storage. While functionalization strategies have red-shifted their absorption profile to harness the solar spectrum more, they also increase molecular weight, thereby reducing gravimetric energy densities to 0.10–0.73 MJ kg^{-1} (*22*–*24*). Similarly, azaborinines offer higher molar energy densities, but require bulky substituents to prevent side reactions such as polymerization, which again compromises gravimetric energy densities (*31*). Furthermore, like many MOST systems reported to date, both norbornadiene and azaborinine operate in solution (*56*, *57*), which significantly lowers their effective gravimetric and volumetric energy densities for fuel applications. Lastly, other areas of material research demonstrate successful incorporation of water-compatible designs (*58*–*61*). In contrast, the general incompatibility of MOST systems with aqueous environments restricts their integration into water-based or environmentally sustainable heating applications.

As a result, there is a critical need for MOST systems that offer high energy density, function under solvent-free conditions (*62*), and incorporate sustainable features such as compatibility with aqueous environments. To address this, we looked to nature for inspiration. A fascinating photochemical process in DNA suggests a new direction for photochemical fuel development. When exposed to high-energy UV light (UV-B/C), nucleobases in DNA can form a derivative of 2-pyrimidone, called a (6-4) lesion (*63*). Further irradiation with lower-energy UV input (UV-A/B) induces the formation of the Dewar isomer. These Dewar lesions are thought to disrupt DNA replication, causing mutations which may lead to cancer (*64*, *65*). Evolution has led to the development of (6-4) photolyase, an enzyme capable of converting the Dewar isomer back into the thermodynamically stable 2-pyrimidone (*63*). Inspired by this reversible Dewar valence isomerization reaction, we became interested in the potential of 2-pyrimidone as a MOST system, along with two related scaffolds, 2-pyridone and 4-pyrimidone.

Derivatives of 2-pyridone and 4-pyrimidone can undergo both forward and reverse Dewar isomerization, but low conversion makes them suboptimal candidates for MOST systems. For example, irreversible [4+4] intermolecular dimerization of 2-pyridone suppresses Dewar formation (*66*, *67*). Dewar isomers of 4-pyrimidones fail to revert quantitatively because of side reactions during thermal activation (*68*, *69*). In contrast, 2-pyrimidone has demonstrated both quantitative photoinduced isomerization and thermally-induced reversion (*70*), making it a more promising scaffold.

In the present study, we report a MOST system based on 2-pyrimidone and its Dewar isomer, engineered for both solvent-free operation and water compatibility. By systematically tuning substituents at the 1-, 4-, and 6-positions of the aromatic core, we optimized energy storage performance while maintaining reversible switching behavior. Notably, our system demonstrates a record-high gravimetric energy density under neat and dilute aqueous conditions, enabling thermal release at a level sufficient to bring water to its boiling point under ambient conditions.

Molecular design

Pyrimidones **1**–**4** (50 mg, 4–20 mM) in acetonitrile (ACN) were irradiated in a photoreactor equipped with commercially available 300-nm lamps. After 24 hours, the formation of the corresponding Dewar isomers was observed. The Dewar isomers were isolated and characterized by ^{1}H and ^{13}C nuclear magnetic resonance (NMR) spectroscopy (figs. S1 to S8), which showed upfield shifts consistent with loss of aromaticity, in agreement with previous reports of pyrimidone valence isomerization (*70*, *71*). We discovered that the Dewar isomers in neat liquid states reverted to their pyrimidone forms when heated above 170°C, confirming the reversibility of the photo–thermal cycle (*vide infra*).

This reversible photoisomerization behavior establishes the pyrimidone/Dewar pair as a viable MOST system. In this system, pyrimidone (P) undergoes valence isomerization to form Dewar (D) isomers, which can be thermally activated to revert to their thermodynamically stable pyrimidone forms, releasing stored energy ($\triangle H_{storage}$) (Fig. 1A). Inspired by the unique aza-bicyclic architecture of DNA lesions, these Dewar isomers fuse highly strained 1,2-dihydroazete (*72*, *73*) and diazetidine (*74*) units, resulting in a compounded strain (*75*). We also strategically incorporated a nitrogen atom at the reaction site, enabling labile C–N bond formation and cleavage (*47*). We hypothesized that this combination of compounded strain and high-energy C–N bond in the Dewar isomer would increase the energy of the metastable state, enhancing $\triangle H_{storage}$ and efficiently controlling thermal release.

To maximize gravimetric energy density, we prioritized lightweight, compact molecular design. Because tautomerization (i.e., keto and enol) competes with the desired photochemical pathway (*76*), the sp^3 secondary nitrogen was methylated to suppress this process. However, attempts to isomerize 1-methyl-2-pyrimidone were unsuccessful, yielding no detectable Dewar isomers via NMR spectroscopy, which was rationalized computationally (*vide infra*). Therefore, to promote efficient valence isomerization while maintaining a

low molecular weight (< 138 g mol^{-1}), additional methyl substituents were introduced to the pyrimidone ring. Three methylated derivatives with distinct substitution patterns, 1,4-dimethyl- (**1**), 1,6-dimethyl- (**2**), and 1,4,6-trimethyl- (**3**) 2-pyrimidones, were synthesized (Fig. 1B). All three compounds can be obtained via one-step nucleophilic substitution or condensation from inexpensive, commercially available precursors. Compound ***3*** was synthesized on a multi-gram scale, highlighting its low cost and potential for commercial scalability.

Although the more compact structures of compounds **1** and **2** were initially expected to deliver superior energy storage performance, compound ***3*** exhibited the highest gravimetric energy storage capacity, establishing the 1,4,6-substitution pattern as optimal. Building on this insight, we designed a liquid-phase derivative, 4,6-dimethyl-1-hexyl-2-pyrimidone (**4**), tailored to undergo isomerization and thermal reversion under solvent-free conditions. All compounds were fully characterized by NMR spectroscopy and high-resolution mass spectrometry (figs. S9 to S16).

Light-induced isomerization of pyrimidones

Our computational mechanistic investigation of the natural orbitals obtained via XMS-CASPT2 calculations of the ground state and Franck-Condon point suggests that the photochemical Dewar isomerization of pyrimidone is initiated by n–π* excitation to the S_1 excited state (figs. S17 and S18). The predicted excitation wavelength for P-***3*** (λ_{cal} = 311 nm) is in good agreement with the experimentally measured absorption maximum (λ_{max} = 307 nm) (fig. S19). When irradiated with a 300-nm or 310-nm lamp, the characteristic n–π* absorption band of P-***3*** decreased over time, indicating the formation of D-***3***, consistent with our NMR characterization. To assess photocharging efficiency, the photoisomerization quantum yields of P-**1** to P-**4** under 310 nm irradiation were measured in ACN and found to range from 0.9% to 7.8% (Fig. 1C, fig. S20, and table S1).

Excited state (XMS-CASPT2, density functional theory (DFT)) calculations indicate that the parent pyrimidone, 1-methyl-2-pyrimidone, exhibits a fast rate of intersystem crossing from the S_1 n–π* surface to the T_1 π–π* excited state ($k_{ISC\ S1\rightarrow T1}$ ~10^{10} s^{-1}), consistent with El Sayed's rule (*77*), followed by rapid ($k_{ISC\ T1\rightarrow S0}$ ~10^{7} s^{-1}) nonradiative decay back to the ground state (fig. S18). As a result, both fluorescence (k_{FL} ~10^{6} s^{-1}) and phosphorescence (k_{phosp} ~10^{1} s^{-1}) are disfavored. This proposes that the prominent nonradiative decay process, rather than photoluminescence, contributes to the low photoisomerization quantum yields. Experimentally measured photoluminescence quantum yield of 0.2% for P-***3*** (Fig. 1C and fig. S21) corroborates this theory.

At present, the pyrimidones that we have studied absorb primarily in the UV-A/B region (~5% of the solar spectrum (*78*)) (Fig. 1D and fig. S19), and the relatively low photoisomerization quantum yields further contribute to the extended charging durations under solar irradiation. To investigate whether future modifications might improve the charging process, we have studied computationally whether substitutions can red-shift the absorption of pyrimidone. Computations summarized in table S2 indicate that introducing a strong donor –NMe_2 at the 4-position or an electron-withdrawer or conjugator –CN and –Ph at the 4- and 6-positions, respectively, will induce a bathochromic shift. These substitutions result in a modest reduction in gravimetric energy density due to the increased molecular weight. Exploration of such compounds in the future is planned.

Pyrimidones **1**–**4** and their Dewar isomers exhibit minimal spectral overlap in the n–π* absorption region (Fig. 1D), enabling high (90–93%) conversion in compounds **1** and **2**, and quantitative conversion (100%) in compounds ***3*** and **4** under continuous irradiation in acetonitrile (figs. S1 to S8). The results were consistent across multiple runs with less than 5% variation in conversion. Importantly, liquid-state P-**4** also underwent effective isomerization under neat conditions (Fig. 1E), eliminating the need for solvent. However, we note that heat release under neat conditions can lead to self-heating (*50*) and potential thermal runaway. We therefore opted to conduct the thermal discharge of the Dewar isomer in organic or aqueous media to ensure controlled heat release. Detailed conditions for energy release in neat and solution states are illustrated in the next section.

To further underscore practicality, we demonstrated the long-term chemical and thermal stability of our pyrimidone over multiple energy storage and release cycles. We aim to create a MOST system capable of storing and releasing heat with total usable energy comparable to conventional heating oil for decentralized residential heating. Conventional heating oil provides heat through a linear, single-use process that involves (1) crude oil extraction, (2) refining, (3) distribution, and (4) combustion (fig. S22A) (*79*, *80*). Each heating cycle consumes the fuel irreversibly, generating (5) greenhouse gas emissions. In contrast, a MOST system, e.g., pyrimidone/Dewar, operates in cycles (fig. S22B, steps ***3.1***–***3.3***). After initial synthesis and distribution to end users, pyrimidone can be charged by light to store energy in its metastable Dewar isomer. The stored energy is retained until heat is required, at which point activation releases the stored heat and regenerates the pyrimidone form. This charge–discharge process is reversible, allowing energy to be extracted multiple times from the same material until performance degradation ultimately necessitates its replacement. Given that the combustion energy of heating oil is approximately 40 MJ kg^{-1} (*3*), a MOST compound storing 1.5–2 MJ kg^{-1} per cycle and operating reversibly for at least 20 cycles could deliver a comparable cumulative thermal output at a similar mass. On this

basis, compound ***3*** was selected for cyclability testing on account of its facile synthesis and representative energy-release performance (*vide infra*).

Charge–discharge cycling of compound ***3*** (5×10^{-5} M, 3 mL) was monitored by UV-Vis spectroscopy (Fig. 1F). Photocharging was carried out by irradiation at 310 nm, while thermal discharge was activated by heating using a temperature-controlled cuvette holder with built-in stirring. To efficiently induce the thermal reversion ($t_{1/2}$ = 481 days at room temperature), the D-***3*** solution was heated to 105°C, the maximum operational temperature of our cuvette holder. As a result, dimethyl sulfoxide (DMSO) was selected to ensure chemical stability and avoid solvent loss during repeated heating (~75 min) and irradiating (~15 min) cycles. Under these conditions, the system showed negligible degradation over more than 20 photoisomerization–thermal reversion cycles in DMSO, confirming the robustness and reversibility.

Remarkable energy storage in Dewar pyrimidones

Pyrimidones exhibit different phase behavior depending on functionalization. Pyrimidones **1**–***3*** are solids at room temperature, whereas pyrimidone **4** is intrinsically liquid per design (Fig. 2A and fig. S23). In contrast, the Dewar isomers generated by irradiating pyrimidones are all obtained as liquids, storing energy. Using differential scanning calorimetry (DSC), we observed and quantified the exothermic heat release ($\Delta H_{storage}$) associated with the D→P reversion in neat conditions. When heated at 10°C min^{-1} from room temperature to above 170°C, Dewar isomers undergo D→P electrocyclic ring-opening, releasing the stored energy ($\Delta H_{storage}$) and generating molten pyrimidones at high temperatures. Pyrimidones ***3***–**4** exhibit excellent thermal stability even at high temperatures, showing negligible thermal decomposition (fig. S24). The NMR spectra of restored pyrimidones after DSC are shown in figs. S25 to S32.

Remarkably, both molecular and gravimetric energy storage densities, measured as exotherms, reach values of 1.65 MJ kg^{-1} or 228 kJ mol^{-1} (Table 1). The storage capacities per mass of the pyrimidone system surpass those of leading photoswitches by at least 160%, including trimeric azaborinine (0.99 MJ kg^{-1} (*81*)), norbornadiene (0.97 MJ kg^{-1} (*26*)), and Dewar anthracene (0.65 MJ kg^{-1} (*32*)) (Fig. 2, B and C). The relevant thermal parameters for the electrocyclic ring-opening processes are summarized in Table 1 and additional physicochemical properties are provided in tables S3 and S4.

The observed outstanding performance of pyrimidones aligned with our hypothesis, confirming the effectiveness of our strategic molecular design. First, the Dewar structure was engineered to experience a compounded strain within the fused bicyclic motif. Second, replacing the traditional C–C bond that is formed and cleaved in MOST systems with a more labile C–N bond enables significantly higher $\Delta H_{storage}$, compared to Dewar anthracene and azaborinine systems that store less than 201 kJ mol^{-1}. Lastly, Dewar isomerization of pyrimidone also results in a complete loss of aromaticity, in contrast to systems such as Dewar anthracene, where aromaticity is only partially disrupted upon photoisomerization (*32*, *53*). Together, these features produce drastically strained and high-energy Dewar pyrimidones, reaching energy storage levels previously inaccessible to MOST systems.

Additionally, we experimentally determined the thermal activation energies ($\Delta H^{\ddagger}$) and extrapolated half-lives ($t_{1/2}$) for the electrocyclic ring-opening of the Dewar isomers in DMSO (figs. S33 to S36 and table S5). The Dewar isomers **2**–**4** demonstrate outstanding thermal stability in solution, with $t_{1/2}$ ranging from months to 3 years (Table 1), despite their high energy states compared to the parent pyrimidones. The long $t_{1/2}$ values highlight their strong potential for durable, long-term energy storage even under fluctuating temperature conditions. We note that the thermal reversion kinetics of D-**1** were not successfully obtained due to side reactions upon heating.

Mechanistic investigations

Our theoretical studies elucidate the photochemical and thermal reaction mechanism of the pyrimidone system (Fig. 3A). Quantum mechanical calculations suggest that Dewar isomerization of P-***3*** proceeds via photon absorption, which initially excites the molecule to the Franck–Condon (FC) n–π* singlet state (fig. S37), which rapidly relaxes to a minimum on the S_1 excited state surface, the adiabatic point (Ad.) This excited state advances to the conical intersection (CI) point, followed by fast decay to the ground state with accompanying heat evolution, forming D-***3***. Pyrimidones **1**, **2**, and **4** follow similar mechanistic pathways, with only minor differences in the energetic profiles (fig. S38). The parent pyrimidone, 1-methyl-2-pyrimidone, displays an energetically elevated FC point (405 kJ mol^{-1}), which potentially accounts for its unsuccessful Dewar isomerization.

Calculation of the 4π-electrocyclic ring-opening reaction coordinate of each pyrimidone highlights the influence of the methyl groups at the 4- and 6-positions on the thermal reversion kinetics of Dewar isomers. Compared to 1-methyl-2-pyrimidone ($\Delta H^{\ddagger}_{cal}$ = 150 kJ mol^{-1}), compounds **2**–**4** bearing a 6-methyl group exhibit a lower $\Delta H^{\ddagger}_{cal}$ (Table 1). Conversely, compound **1**, which features a 4-methyl substituent, displays a higher $\Delta H^{\ddagger}_{cal}$. Furthermore, computational studies on a series of theoretical analogs revealed these substitution effects to be consistent and additive (fig. S39). Our experimental measurements of $\Delta H^{\ddagger}$ and the reversion temperature (T_{rev}) in DSC showed excellent agreement with the theoretical predictions.

We sought to further explore the mechanism behind the observed methyl group substitution effect. Hirshfeld charge

and spin analysis reveal that the 6-methyl substituent lowers the thermal reversion barrier by stabilizing the TS (Fig. 3B). While the TS of 1-methyl-2-pyrimidone exhibits diradical character, that of P-**3** features δ^+ charge accumulation at C6 and zwitterionic character. The polarization of the HONO and LUNO stabilizes the TS, thereby lowering $\Delta H^{\ddagger}_{cal}$ (figs. S40 and S41) (*82*). Natural orbital analysis from multireference calculations (CASSCF) of the two transition states corroborates this observation (fig. S42). Stabilization energy analysis derived from an isodesmic reaction model confirms that the 6-methyl substituent stabilizes the TS more strongly than the Dewar isomer (Fig. 3C). The analysis also finds the 4-methyl group stabilizes the Dewar isomer more than the TS, which in turns increases the $\Delta H^{\ddagger}_{cal}$. We hypothesize that the 4-methyl group contributes to D-**2** stabilization via hyperconjugation (*83*, *84*). The computational details are included in figs. S43 to S45 and table S6.

We then shifted focus to connect our understanding of the reaction thermodynamics to structural mechanistic features of the pyrimidone by constructing a univariate linear free energy relationship. We evaluated the aromaticity of several pyrimidones using the Harmonic Oscillator Model of Aromaticity (HOMA) (Fig. 3D) (*85*, *86*). A clear correlation between increasing aromatic character (1-methyl-2-pyrimidone < P-**1** < P-**3** < P-**2**) and 4π-electrocyclic ring-opening activation energy was observed, indicating progressive stabilization of the pyrimidone ring accelerates thermal reversion. According to the Bell–Evans–Polanyi principle (*87*–*89*), greater stabilization of the ground state pyrimidone leads to a more stabilized TS, thereby lowering the activation barrier (i.e., $\Delta H^{\ddagger}$) to thermal reversion (fig. S46). Taken together, the interplay between aromaticity and the selective effects of the methyl substituents at the 4- and 6-positions explain the trend in both experimental and calculated $\Delta H^{\ddagger}$ values (Table 1).

Calculated energy storage density (ΔH_{cal}) values across the derivatives are generally high, exceeding 200 kJ mol^{-1} (fig. S39). These values are much greater than the experimental $\Delta H_{storage}$ for compounds **1**, **2**, and **4**, but comparable to that of compound **3** (Table 1). We propose that the thermal decomposition of compounds **1** and **2** (figs. S23 and S24) occurs in parallel with the thermally activated reversion pathway, thereby suppressing the overall heat release attainable from the system. The deviation observed in compounds **3** and **4** may be attributed to the different intermolecular interactions. Specifically, compound **4** contains a long hexyl chain, which introduces van der Waals interactions that may disrupt π–π stacking among the parent pyrimidones, thereby destabilizing it. As a result, compound **4** exhibits a lower $\Delta H_{storage}$ than compound **3**, both on a per-mole and per-mass basis.

Despite the lower $\Delta H_{storage}$, compound **4** was specifically tailored for solvent-free operation and a longer energy storage period (3 years vs. 1 year). On the other hand, compound **3**, with its compact structure and high thermal tolerance, delivers record-high energy density of 1.65 MJ kg^{-1} and 228 kJ mol^{-1}.

Heating water with Dewar pyrimidone

MOST systems offer a promising strategy for the controllable capture, storage, and release of solar energy. Over the years, this field has envisioned their integration into a scalable device with a closed-loop architecture (Fig. 4A) (*90*, *91*). In this concept, a MOST compound is dissolved in a circulating solvent that flows through a channel exposed to sunlight. As the solution passes through the illuminated region, the molecules convert from their thermodynamically stable form to a metastable, energy-rich isomer, thereby storing solar energy in chemical bonds. The charged solution is then collected in a reservoir, where the stored energy can be retained for later use. When needed, the solution is directed through a trigger module containing a catalyst embedded within the flow channel. The catalyst triggers the reversion of the metastable isomer to its thermodynamically stable form, releasing the stored energy as heat. This thermal energy is transferred through a heat exchanger to a heat transfer fluid (e.g., cold water), enabling controlled and efficient heat extraction for practical use such as space and water heating.

Herein, we present a simplified proof of concept showing direct heat release and transfer to a typical heat transfer medium, or water. In this experiment, the Dewar isomer, dissolved in water (Fig. 4B), reverts to its pyrimidone form upon triggering, releasing heat to the aqueous solution. To promote the reversion, we employed an acid catalyst, i.e., hydrochloric acid (HCl), which efficiently accelerates the back isomerization (Fig. 4C). This strategy was only made possible by the deliberate incorporation of a nitrogen atom at the bridgehead position of the Dewar isomer (fig. S47). Computations indicate that protonation of the nitrogen lowers $\Delta H^{\ddagger}_{cal}$ by two-fold, thereby enabling spontaneous reversion at room temperature. After heat release, the protonated product can be neutralized to regenerate the original pyrimidone, followed by photo-recharging to form the Dewar isomer. The cyclability of the process was confirmed experimentally (fig. S48).

We note that the use of homogeneous acid catalysts (e.g., HCl) necessitates a neutralization step, leading to salt accumulation that reduces the total energy density. In a practical device configuration, a heterogeneous catalytic process would be preferable, as it would eliminate the need for post–energy-release treatment (*30*). Efforts to develop heterogeneous catalysts to facilitate the electrocyclic ring opening of Dewar pyrimidones represent a promising and important avenue for our future work.

To quantify the heat transfer from D-***3*** to water activated by a catalyst (i.e., HCl), we devised experiment **1**, in which the solution temperature was monitored by infrared (IR) thermal imaging (Fig. 4, B and D). We note that deviations are expected between DSC-measured values ($\triangle H_{DSC}$) and macroscopic IR measurements of heat transferred to a medium ($\triangle H_{IR}$). This is because DSC measurements are performed on neat samples (< 5 mg) under thermally insulated conditions with dynamic heating, whereas acid-catalyzed heat release from D-***3*** (> 50 mg) occurs in a heat-transfer medium, accompanied by heat dissipation to the surroundings.

In experiment **1**, upon addition of HCl (0.5 mmol, 2 M) under ambient conditions, D-***3*** (51 mg in 0.50 mL water) rapidly reverted within 1.8 s, producing a temperature increase ($\triangle T_{IR}$) of 40°C (Fig. 4E). This corresponds to a heat transfer of 85 J ($\triangle H_{IR}$) to the aqueous medium (Fig. 4F and table S7), which is comparable to $\triangle H_{DSC}$ (85 J).

Building on the benchmark experiment **1**, we calculated the amount of D-***3*** needed to boil water. Raising 0.50 mL of water from room temperature to its boiling point ($\triangle T \approx 75$°C) requires approximately 165 J of thermal energy, corresponding to 100 mg of D-***3*** (table S7, entry *calc*). However, boiling of the aqueous solution requires additional energy to overcome the enthalpy of vaporization (2.3 kJ g^{-1} (*92*)). Therefore, the concentration of D-***3*** was slightly increased by employing 107 mg in 0.46 mL of water.

Here, in experiment **2**, we demonstrated that addition of HCl (1.0 mmol, 4.5 M) to D-***3*** solution raised the solution temperature to 100°C and induced boiling within 1 s (movie S1). IR thermal imaging measured a $\triangle T_{IR}$ of 76°C, corresponding to a $\triangle H_{IR}$ of 153 J transferred to the aqueous solution (Fig. 4, E and F), whereas 107 mg of D-***3*** is expected to release 176 J ($\triangle H_{DSC}$). We therefore attribute the energy difference ($\triangle\triangle H$ = 23 J) to the boiling process, an amount sufficient to vaporize approximately 10 μL (2.2%) of water. After reaching the initial peak, the water temperature decreased gradually (movie S1).

We note that additional exotherm from the protonation process contributes to the measured heat transfer ($\triangle H_{IR}$) in experiments **1** and **2**. To quantify the exotherm, we performed a control experiment ***3*** where P-***3*** (106 mg in 0.46 mL water) was protonated to increase the temperature only by 7°C, corresponding to 14 J of heat transfer (Fig. 4, E and F). This confirms that the substantial total heat transfer observed in experiments **1** and **2** primarily originates from the energy released from the reverse Dewar isomerization rather than from protonation.

Previously, quadricyclanes were shown to release heat in highly controlled experiments employing a thermally insulated vacuum chamber to minimize heat loss (*90*). In such experiments, a solution of quadricyclane (1.5 M) in toluene was continuously flowed (5 mL h^{-1}) through a catalytic channel consisting of cobalt phthalocyanine on an alumina surface. The reversion induced a maximum temperature increase of 63°C after 2.5 min. Under these conditions, approximately 70 mg of quadricyclane transferred 27 J of thermal energy to 0.21 mL of solution, corresponding to a normalized transferred energy of 0.38 MJ kg^{-1}, which is comparable to the energy density measured by DSC (0.40 MJ kg^{-1}). In our work, D-***3*** with a substantially higher energy density (1.65 MJ kg^{-1}) enables rapid heating and boiling of water under ambient conditions at comparable or lower concentrations.

Beyond quadricyclanes catalyzed by metal complexes, we also performed acid-catalyzed heat-release experiments using other representative MOST compounds, namely diazetidine and *cis*-azobenzene (Fig. 4D, experiments **4** and **5**). Because both diazetidine and *cis*-azobenzene are poorly soluble in water, benzene was used as the heat-transfer medium, and trifluoroacetic acid (1.0 mmol, 4.5 M) was employed as the catalyst. Under comparable mass loadings (~106 mg), D-***3*** transferred substantially more heat (153 J) to the medium than diazetidine (14 J) and *cis*-azobenzene (11 J) (Fig. 4F). This trend is consistent with the higher gravimetric energy density of D-***3*** (1.65 MJ kg^{-1}) than those of diazetidine (0.32 MJ kg^{-1}) and *cis*-azobenzene (0.23 MJ kg^{-1}) (table S7). The heat-release processes and the NMR analysis confirming complete reversions are illustrated in detail in movies S2 to S5 and figs. S49 to S56.

We note that benzene has a lower heat capacity (1.7 J g^{-1} K^{-1}) than water (4.2 J g^{-1} K^{-1}) (*93*, *94*). Therefore, diazetidine and *cis*-azobenzene reach maximum temperatures of 42°C and 34°C, respectively, despite transferring only 14 J and 11 J of energy to the medium (Fig. 4, E and F, experiments **4** and **5**). Based on these results, we conclude that the maximum attainable temperature of the medium is governed by three parameters: (i) the gravimetric energy density of the MOST compound, (ii) the heat capacity of the medium, and (iii) the mass of the MOST compound dissolved (Fig. 4G).

Moreover, the difference between the released enthalpy measured by DSC and the heat transferred to the medium ($\triangle\triangle H = \triangle H_{DSC} - \triangle H_{IR}$) is substantial for diazetidine and *cis*-azobenzene (Fig. 4F, experiments **4** and **5**) despite the absence of boiling. Specifically, only 42% and 48% of the released energy was delivered to the medium for diazetidine and *cis*-azobenzene, respectively (table S7). These results suggest that, even under similar experimental conditions, the heat-transfer efficiency ($\triangle H_{IR}/\triangle H_{DSC}$) depends strongly on the reaction rate. For diazetidine, which is initially insoluble in benzene and slowly dissolves upon protonation (fig. S49), it takes 7.6 s to reach the maximum temperature during the heat release and transfer, thereby subject to greater heat loss to the surroundings (Fig. 4E). In the case of *cis*-azobenzene, despite its high solubility, the protonation and heat-release process appear to be slower (2.4 s) than those of Dewar

pyrimidone, which similarly contributes to heat loss to the surroundings during heat release and transfer. Therefore, we propose that both (i) solubility and (ii) reaction rate are important factors influencing heat-transfer efficiency under ambient conditions (Fig. 4G).

Overall, we show that high energy-density Dewar pyrimidone (1.65 MJ kg^{-1}) can be efficiently catalyzed to release its stored heat and transfer it to an environmentally benign medium such as water (Fig. 4H). Although this proof-of-concept experiment has not yet been optimized, it highlights the potential of this molecular fuel for practical heating applications. Future work will focus on integrating heterogeneous catalysts immobilized within the channel near a heat exchanger (Fig. 4A), allowing the Dewar solution to flow through and be activated in situ without the need for post–heat-release treatment prior to recharging. The released heat can be extracted through a heat exchanger and delivered to a heat-transfer fluid (e.g., water) for heating applications.

Conclusions

In this work, we developed a pyrimidone-based MOST system guided by two key principles: i) the incorporation of a highly strained, dearomatized aza-bicyclic scaffold to maximize stored energy and ii) nitrogen incorporated at the reactive site to provide precise control over thermal release. Together, these features yielded a compact molecular architecture with an energy density of 1.65 MJ kg^{-1}. As a proof-of-concept, we demonstrated heat delivery sufficient to boil 0.46 mL (460 mg) of water using 107 mg of a MOST material. This result marks an important step in advancing molecular solar thermal technologies from concepts to practical, scalable solutions for water heating, cooking, and surface defrosting in everyday settings.

Materials and methods are available in the supplementary materials.

REFERENCES AND NOTES

1. IRENA, IEA, REN21, "Renewable Energy Policies in a Time of Transition: Heating and Cooling" (2020); https://www.irena.org/publications/2020/Nov/Renewable-Energy-Policies-in-a-Time-of-Transition-Heating-and-Cooling.
2. International Energy Agency (IEA), Heating (2023); https://www.iea.org/energy-system/buildings/heating.
3. Alternative Fuels Data Center, Fuel Properties Comparison; https://afdc.energy.gov/fuels/properties.
4. R. Götz, R. Streng, J. Sterzinger, T. Steeger, M. M. Kaye, M. Vitort, A. S. Bandarenka, All-solid-state Li-ion batteries with commercially available electrolytes: A feasibility review. *InfoMat* **6**, e12627 (2024). doi:10.1002/inf2.12627
5. M. U. Farid, J. A. Kharraz, S. Sharma, R. J. Khan, N. K. Khanzada, B. J. Deka, M. K. Nallapaneni, S. S. Chopra, S.-Y. Leu, S. W. Hasan, N. Hilal, A. K. J. An, Technological advancements in water heating approaches for membrane distillation desalination process: From bulk to localized heating. *Desalination* **574**, 117235 (2024). doi:10.1016/j.desal.2023.117235
6. G. R. Gossweiler, C. L. Brown, G. B. Hewage, E. Sapiro-Gheiler, W. J. Trautman, G. W. Welshofer, S. L. Craig, Mechanochemically Active Soft Robots. *ACS Appl. Mater. Interfaces* **7**, 22431–22435 (2015). doi:10.1021/acsami.5b06440 Medline
7. Z. S. Kean, S. Akbulatov, Y. Tian, R. A. Widenhoefer, R. Boulatov, S. L. Craig, Photomechanical actuation of ligand geometry in enantioselective catalysis. *Angew. Chem. Int. Ed.* **53**, 14508–14511 (2014). doi:10.1002/anie.201407494 Medline
8. A. M. Alfaraidi, B. Kudisch, N. Ni, J. Thomas, T. Y. George, K. Rajabimoghadam, H. J. Jiang, D. G. Nocera, M. J. Aziz, R. Y. Liu, Reversible CO_2 Capture and On-Demand Release by an Acidity-Matched Organic Photoswitch. *J. Am. Chem. Soc.* **145**, 26720–26727 (2023). doi:10.1021/jacs.3c08471 Medline
9. P. Wójcik, T. Khvorost, G. Lao, G.-Z. Zhu, A. Macias Jr., J. R. Caram, W. C. Campbell, M. A. García-Garibay, E. R. Hudson, A. N. Alexandrova, A. I. Krylov, Photoswitching Molecules Functionalized with Optical Cycling Centers Provide a Novel Platform for Studying Chemical Transformations in Ultracold Molecules. *J. Phys. Chem. A* **129**, 1929–1940 (2025). doi:10.1021/acs.jpca.4c06320 Medline
10. A. Siiskonen, S. Vesamäki, A. Priimagi, Azobenzene protonation as a tool for temperature sensing. *Beilstein J. Org. Chem.* **21**, 1528–1534 (2025). doi:10.3762/bjoc.21.115 Medline
11. C. M. Tobin, R. Gordon, S. K. Tochikura, B. F. Chmelka, D. E. Morse, J. Read de Alaniz, Reversible and size-controlled assembly of reflectin proteins using a charged azobenzene photoswitch. *Chem. Sci.* **15**, 13279–13289 (2024). doi:10.1039/D4SC03299C Medline
12. T. Wachsmuth, R. Kluifhooft, M. Müller, L. Zeiß, M. Kathan, A molecular machine directs the synthesis of a catenane. *Science* **389**, 526–531 (2025). doi:10.1126/science.adx5363 Medline
13. L. Dong, Y. Feng, L. Wang, W. Feng, Azobenzene-based solar thermal fuels: Design, properties, and applications. *Chem. Soc. Rev.* **47**, 7339–7368 (2018). doi:10.1039/C8CS00470F Medline
14. R. Losantos, D. Sampedro, Design and Tuning of Photoswitches for Solar Energy Storage. *Molecules* **26**, 3796 (2021). doi:10.3390/molecules26133796 Medline
15. Q. Qiu, S. Yang, M. A. Gerkman, H. Fu, I. Aprahamian, G. G. D. Han, Photon Energy Storage in Strained Cyclic Hydrazones: Emerging Molecular Solar Thermal Energy Storage Compounds. *J. Am. Chem. Soc.* **144**, 12627–12631 (2022). doi:10.1021/jacs.2c05384 Medline
16. Z. Wang, J. Udmark, K. Börjesson, R. Rodrigues, A. Roffey, M. Abrahamsson, M. B. Nielsen, K. Moth-Poulsen, Evaluating Dihydroazulene/Vinylheptafulvene Photoswitches for Solar Energy Storage Applications. *ChemSusChem* **10**, 3049–3055 (2017). doi:10.1002/cssc.201700679 Medline
17. M. Brøndsted Nielsen, N. Ree, K. V. Mikkelsen, M. Cacciarini, Tuning the dihydroazulene – vinylheptafulvene couple for storage of solar energy. *Russ. Chem. Rev.* **89**, 573–586 (2020). doi:10.1070/RCR4944
18. A. Lennartson, A. Lundin, K. Börjesson, V. Gray, K. Moth-Poulsen, Tuning the photochemical properties of the fulvalene-tetracarbonyl-diruthenium system. *Dalton Trans.* **45**, 8740–8744 (2016). doi:10.1039/C6DT01343K Medline
19. K. Börjesson, D. Ćoso, V. Gray, J. C. Grossman, J. Guan, C. B. Harris, N. Hertkorn, Z. Hou, Y. Kanai, D. Lee, J. P. Lomont, A. Majumdar, S. K. Meier, K. Moth-Poulsen, R. L. Myrabo, S. C. Nguyen, R. A. Segalman, V. Srinivasan, W. B. Tolman, N. Vinokurov, K. P. C. Vollhardt, T. W. Weidman, Exploring the potential of fulvalene dimetals as platforms for molecular solar thermal energy storage: Computations, syntheses, structures, kinetics, and catalysis. *Chemistry* **20**, 15587–15604 (2014). doi:10.1002/chem.201404170 Medline
20. Y. Kanai, V. Srinivasan, S. K. Meier, K. P. C. Vollhardt, J. C. Grossman, Mechanism of thermal reversal of the (fulvalene)tetracarbonyldiruthenium photoisomerization: Toward molecular solar-thermal energy storage. *Angew. Chem. Int. Ed.* **49**, 8926–8929 (2010). doi:10.1002/anie.201002994 Medline
21. R. R. Weber, C. N. Stindt, A. M. J. van der Harten, B. L. Feringa, Push-Pull Bis-Norbornadienes for Solar Thermal Energy Storage. *Chemistry* **30**, e202400482 (2024). doi:10.1002/chem.202400482 Medline
22. K. Jorner, A. Dreos, R. Emanuelsson, O. El Bakouri, I. F. Galván, K. Börjesson, F. Feixas, R. Lindh, B. Zietz, K. Moth-Poulsen, H. Ottosson, Unraveling factors leading to efficient norbornadiene–quadricyclane molecular solar-thermal energy storage systems. *J. Mater. Chem. A* **5**, 12369–12378 (2017). doi:10.1039/C7TA04259K
23. R. Schulte, S. Afflerbach, T. Paululat, H. Ihmels, Bis- and Tris-norbornadienes with High Energy Densities for Efficient Molecular Solar Thermal Energy Storage. *Angew. Chem. Int. Ed.* **62**, e202309544 (2023). doi:10.1002/anie.202309544 Medline
24. L. Fei, H. Hölzel, Z. Wang, A. E. Hillers-Bendtsen, A. S. Aslam, M. Shamsabadi, J. Tan, K. V. Mikkelsen, C. Wang, K. Moth-Poulsen, Two-way photoswitching

norbornadiene derivatives for solar energy storage. *Chem. Sci.* **15**, 18179–18186 (2024). doi:10.1039/D4SC04247F Medline
25. M. Mansø, A. U. Petersen, Z. Wang, P. Erhart, M. B. Nielsen, K. Moth-Poulsen, Molecular solar thermal energy storage in photoswitch oligomers increases energy densities and storage times. *Nat. Commun.* **9**, 1945 (2018). doi:10.1038/s41467-018-04230-8 Medline
26. X. An, Y. Xie, Enthalpy of isomerization of quadricyclane to norbornadiene. *Thermochim. Acta* **220**, 17–25 (1993). doi:10.1016/0040-6031(93)80451-F
27. A. U. Petersen, A. I. Hofmann, M. Fillols, M. Mansø, M. Jevric, Z. Wang, C. J. Sumby, C. Müller, K. Moth-Poulsen, Solar Energy Storage by Molecular Norbornadiene-Quadricyclane Photoswitches: Polymer Film Devices. *Adv. Sci.* **6**, 1900367 (2019). doi:10.1002/advs.201900367 Medline
28. M. Quant, A. Lennartson, A. Dreos, M. Kuisma, P. Erhart, K. Börjesson, K. Moth-Poulsen, Low Molecular Weight Norbornadiene Derivatives for Molecular Solar-Thermal Energy Storage. *Chemistry* **22**, 13265–13274 (2016). doi:10.1002/chem.201602530 Medline
29. M. Quant, A. E. Hillers-Bendtsen, S. Ghasemi, M. Erdelyi, Z. Wang, L. M. Muhammad, N. Kann, K. V. Mikkelsen, K. Moth-Poulsen, Synthesis, characterization and computational evaluation of bicyclooctadienes towards molecular solar thermal energy storage. *Chem. Sci.* **13**, 834–841 (2021). doi:10.1039/D1SC05791J Medline
30. Z. Hussain, R. Einholz, S. M. Biebl, E. Franz, A. Müller, A. Dreuw, H. F. Bettinger, O. Brummel, J. Libuda, Heterogeneously Catalyzed Energy Release in Azaborinine-based Molecular Solar Thermal Systems. *Top. Catal.* **68**, 1883–1891 (2025). doi:10.1007/s11244-025-02089-w
31. K. Edel, X. Yang, J. S. A. Ishibashi, A. N. Lamm, C. Maichle-Mössmer, Z. X. Giustra, S.-Y. Liu, H. F. Bettinger, The Dewar Isomer of 1,2-Dihydro-1,2-azaborinines: Isolation, Fragmentation, and Energy Storage. *Angew. Chem. Int. Ed.* **57**, 5296–5300 (2018). doi:10.1002/anie.201712683 Medline
32. S. Chakraborty, W. S. R. Choudhuri, J. Usuba, Q. Qiu, C. Raju, G. G. D. Han, Curved anthracenes for visible-light photon energy storage via Dewar isomerization. *Chem* **11**, 102660 (2025). doi:10.1016/j.chempr.2025.102660 Medline
33. S. Helmy, F. A. Leibfarth, S. Oh, J. E. Poelma, C. J. Hawker, J. Read de Alaniz, Photoswitching using visible light: A new class of organic photochromic molecules. *J. Am. Chem. Soc.* **136**, 8169–8172 (2014). doi:10.1021/ja503016b Medline
34. J. Gemen, J. R. Church, T.-P. Ruoko, N. Durandin, M. J. Białek, M. Weißenfels, M. Feller, M. Kazes, M. Odaybat, V. A. Borin, R. Kalepu, Y. Diskin-Posner, D. Oron, M. J. Fuchter, A. Priimagi, I. Schapiro, R. Klajn, Disequilibrating azobenzenes by visible-light sensitization under confinement. *Science* **381**, 1357–1363 (2023). doi:10.1126/science.adh9059 Medline
35. G. C. Thaggard, K. C. Park, J. Lim, B. K. P. Maldeni Kankanamalage, J. Haimerl, G. R. Wilson, M. K. McBride, K. L. Forrester, E. R. Adelson, V. S. Arnold, S. T. Wetthasinghe, V. A. Rassolov, M. D. Smith, D. Sosnin, I. Aprahamian, M. Karmakar, S. K. Bag, A. Thakur, M. Zhang, B. Z. Tang, J. A. Castaño, M. N. Chaur, M. M. Lerch, R. A. Fischer, J. Aizenberg, R. Herges, J.-M. Lehn, N. B. Shustova, Breaking the photoswitch speed limit. *Nat. Commun.* **14**, 7556 (2023). doi:10.1038/s41467-023-43405-w Medline
36. J. Haimerl, G. C. Thaggard, B. K. P. Maldeni Kankanamalage, R. Bühler, J. Lim, K. C. Park, J. Warnan, R. A. Fischer, N. B. Shustova, Shifting Gears: Photochromic Metal-Organic Frameworks with Stimulus-Adaptable Performance. *J. Am. Chem. Soc.* **147**, 19918–19930 (2025). doi:10.1021/jacs.5c04466 Medline
37. A. D. W. Kennedy, I. Sandler, J. Andréasson, J. Ho, J. E. Beves, Visible-Light Photoswitching by Azobenzazoles. *Chemistry* **26**, 1103–1110 (2020). doi:10.1002/chem.201904309 Medline
38. H. Qian, S. Pramanik, I. Aprahamian, Photochromic Hydrazone Switches with Extremely Long Thermal Half-Lives. *J. Am. Chem. Soc.* **139**, 9140–9143 (2017). doi:10.1021/jacs.7b04993 Medline
39. B. Shao, H. Fu, I. Aprahamian, A molecular anion pump. *Science* **385**, 544–549 (2024). doi:10.1126/science.adp3506 Medline
40. D. Kolarski, P. Steinbach, C. Bannwarth, K. Klaue, S. Hecht, Diaryltriazolium Photoswitch: Reaching a Millisecond Cycloreversion with High Stability and NIR Absorption. *Angew. Chem. Int. Ed.* **63**, e202318015 (2024). doi:10.1002/anie.202318015
41. J. Wu, L. Kreimendahl, J. L. Greenfield, Enhancing the Photoswitching Properties of *N*-Alkyl Imines. *J. Am. Chem. Soc.* **147**, 17549–17554 (2025). doi:10.1021/jacs.5c02404 Medline
42. M. Purdy, A. Y. Wang, M. C. Drummer, D. G. Nocera, R. Y. Liu, Reversible fluorenol photobases that perform CO_2 capture and concentration from ambient air. *Nat. Chem.* **17**, 1680–1687 (2025). doi:10.1038/s41557-025-01901-0 Medline
43. K. Kuntze, D. R. S. Pooler, M. Di Donato, M. F. Hilbers, P. van der Meulen, W. J. Buma, A. Priimagi, B. L. Feringa, S. Crespi, A visible-light-driven molecular motor based on barbituric acid. *Chem. Sci.* **14**, 8458–8465 (2023). doi:10.1039/D3SC03090C Medline
44. J. Calbo, C. E. Weston, A. J. P. White, H. S. Rzepa, J. Contreras-García, M. J. Fuchter, Tuning Azoheteroarene Photoswitch Performance through Heteroaryl Design. *J. Am. Chem. Soc.* **139**, 1261–1274 (2017). doi:10.1021/jacs.6b11626 Medline
45. N. J. Oldenhuis, K. P. Qin, S. Wang, H.-Z. Ye, E. A. Alt, A. P. Willard, T. Van Voorhis, S. L. Craig, J. A. Johnson, Photoswitchable Sol-Gel Transitions and Catalysis Mediated by Polymer Networks with Coumarin-Decorated Cu_{24} L_{24} Metal-Organic Cages as Junctions. *Angew. Chem. Int. Ed.* **59**, 2784–2792 (2020). doi:10.1002/anie.201913297 Medline
46. J. Wang, L. Avram, Y. Diskin-Posner, M. J. Białek, W. Stawski, M. Feller, R. Klajn, Altering the Properties of Spiropyran Switches Using Coordination Cages with Different Symmetries. *J. Am. Chem. Soc.* **144**, 21244–21254 (2022). doi:10.1021/jacs.2c08901 Medline
47. H. P. Q. Nguyen, A. Mukherjee, J. Usuba, J. Wan, G. G. D. Han, Large and long-term photon energy storage in diazetidines *via* [2+2] photocycloaddition. *Chem. Sci.* **15**, 18846–18854 (2024). doi:10.1039/D4SC05374E Medline
48. M. A. Gerkman, R. S. L. Gibson, J. Calbo, Y. Shi, M. J. Fuchter, G. G. D. Han, Arylazopyrazoles for Long-Term Thermal Energy Storage and Optically Triggered Heat Release below 0 °C. *J. Am. Chem. Soc.* **142**, 8688–8695 (2020). doi:10.1021/jacs.0c00374 Medline
49. Y. Shi, M. A. Gerkman, Q. Qiu, S. Zhang, G. G. D. Han, Sunlight-activated phase change materials for controlled heat storage and triggered release. *J. Mater. Chem. A* **9**, 9798–9808 (2021). doi:10.1039/D1TA01007G
50. S. Chakraborty, H. P. Q. Nguyen, J. Usuba, J. Y. Choi, Z. Sun, C. Raju, G. Sigelmann, Q. Qiu, S. Cho, S. M. Tenney, K. E. Shulenberger, K. Schmidt-Rohr, J. Park, G. G. D. Han, Self-activated energy release cascade from anthracene-based solid-state molecular solar thermal energy storage systems. *Chem* **10**, 3309–3322 (2024). doi:10.1016/j.chempr.2024.06.033 Medline
51. A. Giménez-Gómez, L. Magson, C. Merino-Robledillo, S. Hernáez-Troya, N. Sanosa, D. Sampedro, I. Funes-Ardoiz, State-of-the-art and challenges towards a Molecular Solar Thermal (MOST) energy storage device. *React. Chem. Eng.* **9**, 1629–1640 (2024). doi:10.1039/D4RE00131A
52. H. F. Bettinger, O. Hauler, Ring opening of 2-aza-3-borabicyclo[2.2.0]hex-5-ene, the Dewar form of 1,2-dihydro-1,2-azaborine: Stepwise versus concerted mechanisms. *Beilstein J. Org. Chem.* **9**, 761–766 (2013). doi:10.3762/bjoc.9.86 Medline
53. P. von Ragué Schleyer, M. Manoharan, H. Jiao, F. Stahl, The acenes: Is there a relationship between aromatic stabilization and reactivity? *Org. Lett.* **3**, 3643–3646 (2001). doi:10.1021/ol016553b Medline
54. A. T. Balaban, Pv. Schleyer, H. S. Rzepa, Crocker, not Armit and Robinson, begat the six aromatic electrons. *Chem. Rev.* **105**, 3436–3447 (2005). doi:10.1021/cr0300946 Medline
55. US Food and Drug Administration, Ultraviolet (UV) Radiation (2020); https://www.fda.gov/radiation-emitting-products/tanning/ultraviolet-uv-radiation#UVCrisks.
56. F. Hemauer, H.-P. Steinrück, C. Papp, The Norbornadiene/Quadricyclane Pair as Molecular Solar Thermal Energy Storage System: Surface Science Investigations. *Chemphyschem* **25**, e202300806 (2024). doi:10.1002/cphc.202300806 Medline
57. R. C. Richter, S. M. Biebl, R. Einholz, J. Walz, C. Maichle-Mössmer, M. Ströbele, H. F. Bettinger, I. Fleischer, Facile Energy Release from Substituted Dewar Isomers of 1,2-Dihydro-1,2-Azaborinines Catalyzed by Coinage Metal Lewis Acids. *Angew. Chem. Int. Ed.* **63**, e202405818 (2024). doi:10.1002/anie.202405818 Medline
58. G. C. Thaggard, N. B. Shustova, COFs in the Game: Harvest Water to Sustain. *ACS Cent. Sci.* **11**, 653–655 (2025). doi:10.1021/acscentsci.5c00357 Medline
59. A. M. Alfaraidi, D. Xi, N. Ni, T. Y. George, T. Tsukamoto, R. G. Gordon, M. J. Aziz, R.

Y. Liu, An Extremely Stable and Soluble NH_2-Substituted Anthraquinone Electrolyte for Aqueous Redox Flow Batteries. *ACS Appl. Energy Mater.* **6**, 12259–12266 (2023). doi:10.1021/acsaem.3c01943
60. P. Lentes, P. Frühwirt, H. Freißmuth, W. Moormann, F. Kruse, G. Gescheidt, R. Herges, Photoswitching of Diazocines in Aqueous Media. *J. Org. Chem.* **86**, 4355–4360 (2021). doi:10.1021/acs.joc.1c00065 Medline
61. P. Commins, M. A. Garcia-Garibay, Photochromic molecular gyroscope with solid state rotational states determined by an azobenzene bridge. *J. Org. Chem.* **79**, 1611–1619 (2014). doi:10.1021/jo402516n Medline
62. N. B. Shustova, Anthracene-based energy storage. *Joule* **8**, 2957–2959 (2024). doi:10.1016/j.joule.2024.10.015
63. J. Yamamoto, P. Plaza, K. Brettel, Repair of (6-4) Lesions in DNA by (6-4) Photolyase: 20 Years of Quest for the Photoreaction Mechanism. *Photochem. Photobiol.* **93**, 51–66 (2017). doi:10.1111/php.12696 Medline
64. D. Perdiz, P. Gróf, M. Mezzina, O. Nikaido, E. Moustacchi, E. Sage, Distribution and repair of bipyrimidine photoproducts in solar UV-irradiated mammalian cells. *J. Biol. Chem.* **275**, 26732–26742 (2000). doi:10.1016/S0021-9258(19)61437-7 Medline
65. T. Douki, A. Reynaud-Angelin, J. Cadet, E. Sage, Bipyrimidine photoproducts rather than oxidative lesions are the main type of DNA damage involved in the genotoxic effect of solar UVA radiation. *Biochemistry* **42**, 9221–9226 (2003). doi:10.1021/bi034593c Medline
66. R. C. De Selms, W. R. Schleigh, Heterocyclodieneone photochemistry I. Photo-2-pyridone (2-aza-3-oxobicyclo[2.2.0]hex-5-ene). *Tetrahedron Lett.* **13**, 3563–3566 (1972). doi:10.1016/S0040-4039(01)94100-0
67. W. A. Ayer, R. Hayatsu, P. de Mayo, S. T. Reid, J. B. Stothers, The photodimers of α-pyridones. *Tetrahedron Lett.* **2**, 648–653 (1961). doi:10.1016/S0040-4039(01)91666-1
68. S. Hirokami, T. Takahashi, M. Nagata, T. Yamazaki, Rearrangements of Dewar 4-pyrimidinones and 4-methoxy-2-azetidinones. Reactions through azetidinyl and acyl cations. *J. Org. Chem.* **52**, 2455–2468 (1987). doi:10.1021/jo00388a022
69. S. I. Hirokami Si, A. Murao, H. Kakuda, H. Shinoda, Y. Koga, X-ray Crystal Structures and ab Initio Calculations on the Photochemically Formed Dewar Isomers of the 4(3*H*)-Pyrimidinone Derivatives. *J. Org. Chem.* **62**, 2711–2719 (1997). doi:10.1021/jo962103z Medline
70. T. Nishio, A. Kato, C. Kashima, Y. Omote, Photochemical electrocyclization of 1,4,6-trisubstituted pyrimidin-2-ones to 2-oxo-1,3-diazabicyclo[2.2.0]hex-5-enes. *J. Chem. Soc. Perkin Trans. 1* **1980**, 607–610 (1980). doi:10.1039/p19800000607
71. J. S. Taylor, D. S. Garrett, M. P. Cohrs, Solution-state structure of the Dewar pyrimidinone photoproduct of thymidylyl-(3′.fwdarw. 5′)-thymidine. *Biochemistry* **27**, 7206–7215 (1988). doi:10.1021/bi00419a007 Medline
72. S. A. Smith, Q. Cheng, G. Hill, D. H. Magers, Conventional strain energies of 1,2-dihydroazete, 2,3-dihydroazete, 1,2-dihydrophosphete, and 2,3-dihydrophosphete. *Struct. Chem.* **24**, 1681–1691 (2013). doi:10.1007/s11224-012-0186-9
73. G. W. Breton, K. L. Martin, Are 1,2-dihydrodiazetes aromatic? An experimental and computational investigation. *J. Org. Chem.* **67**, 6699–6704 (2002). doi:10.1021/jo026082m Medline
74. L. E. Gusel'nikov, V. G. Avakyan, S. L. Guselnikov, Hetero-π-systems from 2 + 2 cycloreversion, part 2. [1]Ab initio thermochemical study of heterocyclobutanes 2 + 2 cycloreversion to form heteroethenes H_2C=X (X=NH, O, SiH_2, PH, S). *Heteroatom Chem.* **18**, 704–720 (2007). doi:10.1002/hc.20377
75. K. B. Wiberg, G. Bonneville, R. Dempsey, Strain Energies of Small Ring Alkenes. *Isr. J. Chem.* **23**, 85–92 (1983). doi:10.1002/ijch.198300011
76. L. Lapinski, M. J. Nowak, A. Les, L. Adamowicz, Ab Initio Calculations of IR Spectra in Identification of Products of Matrix Isolation Photochemistry: Dewar Form of 4(3H)-Pyrimidinone. *J. Am. Chem. Soc.* **116**, 1461–1467 (1994). doi:10.1021/ja00083a035
77. M. A. El-Sayed, Triplet state. Its radiative and nonradiative properties. *Acc. Chem. Res.* **1**, 8–16 (1968). doi:10.1021/ar50001a002
78. ASTM International, "Standard Tables for Reference Solar Spectral Irradiances: Direct Normal and Hemispherical on 37° Tilted Surface" (ASTM G173-23, 2023); https://store.astm.org/g0173-23.html.
79. University of Wisconsin–Green Bay, "Heating Fuel Life-cycle Assessment" (Pellet Fuels Institute, Final Report, 2007); https://www.pelletheat.org/assets/docs/industry-data/final-pfi-study.pdf.
80. N. Jungbluth, P. Wenzel, C. Meili, "Life cycle inventories of oil heating systems: Final report" (ESU-services Ltd., 2018); https://esu-services.ch/fileadmin/download/publicLCI/jungbluth-2018_LCI_of_oil_heating_systems.pdf.
81. S. M. Biebl, R. C. Richter, M. Ströbele, I. Fleischer, H. F. Bettinger, High energy density dihydroazaborinine dyads and triad for molecular solar thermal energy storage. *Chem. Sci.* **16**, 15231–15238 (2025). doi:10.1039/D5SC03159A Medline
82. G. A. Kukier, A. Turlik, X.-S. Xue, K. N. Houk, Violations. How Nature Circumvents the Woodward–Hoffmann Rules and Promotes the Forbidden Conrotatory 4*n* + 2 Electron Electrocyclization of Prinzbach's Vinylogous Sesquifulvalene. *J. Am. Chem. Soc.* **143**, 21694–21704 (2021). doi:10.1021/jacs.1c11058 Medline
83. H. M. Frey, B. M. Pope, R. F. Skinner, Thermal isomerization of cyclobutenes. Part 10.—3,3-Dimethylcyclobutene and 1,3,3-trimethylcyclobutene. *Trans. Faraday Soc.* **63**, 1166–1170 (1967). doi:10.1039/TF9676301166
84. P. Nava, Y. Carissan, On the ring-opening of substituted cyclobutene to benzocyclobutene: Analysis of π delocalization, hyperconjugation, and ring strain. *Phys. Chem. Chem. Phys.* **16**, 16196–16203 (2014). doi:10.1039/C4CP01695E Medline
85. J. Kruszewski, T. M. Krygowski, Definition of aromaticity basing on the harmonic oscillator model. *Tetrahedron Lett.* **13**, 3839–3842 (1972). doi:10.1016/S0040-4039(01)94175-9
86. T. M. Krygowski, Crystallographic studies of inter- and intramolecular interactions reflected in aromatic character of. pi.-electron systems. *J. Chem. Inf. Comput. Sci.* **33**, 70–78 (1993). doi:10.1021/ci00011a011
87. M. G. Evans, M. Polanyi, Inertia and driving force of chemical reactions. *Trans. Faraday Soc.* **34**, 11–24 (1938). doi:10.1039/tf9383400011
88. J. N. Bronsted, Acid and Basic Catalysis. *Chem. Rev.* **5**, 231–338 (1928). doi:10.1021/cr60019a001
89. R. P. Bell, The theory of reactions involving proton transfers. *Proc. A* **154**, 414–429 (1997). doi:10.1098/rspa.1936.0060
90. Z. Wang, A. Roffey, R. Losantos, A. Lennartson, M. Jevric, A. U. Petersen, M. Quant, A. Dreos, X. Wen, D. Sampedro, K. Börjesson, K. Moth-Poulsen, Macroscopic heat release in a molecular solar thermal energy storage system. *Energy Environ. Sci.* **12**, 187–193 (2019). doi:10.1039/C8EE01011K
91. K. Moth-Poulsen, D. Ćoso, K. Börjesson, N. Vinokurov, S. K. Meier, A. Majumdar, K. P. C. Vollhardt, R. A. Segalman, Molecular solar thermal (MOST) energy storage and release system. *Energy Environ. Sci.* **5**, 8534–8537 (2012). doi:10.1039/c2ee22426g
92. D. R. Lide Ed., *CRC Handbook of Chemistry and Physics* (CRC Press, ed. 84, 2004).
93. N. H. Almousa, M. R. Alotaibi, M. Alsohybani, D. Radziszewski, S. M. AlNoman, B. M. Alotaibi, M. M. Khayyat, Paraffin Wax [As a Phase Changing Material (PCM)] Based Composites Containing Multi-Walled Carbon Nanotubes for Thermal Energy Storage (TES) Development. *Crystals* **11**, 951 (2021). doi:10.3390/cryst11080951
94. J. P. E. Grolier, G. Roux-Desgranges, M. Berkane, E. Jiménez, E. Wilhelm, Heat capacities and densities of mixtures of very polar substances 2. Mixtures containing *N*, *N*-dimethylformamide. *J. Chem. Thermodyn.* **25**, 41–50 (1993). doi:10.1006/jcht.1993.1005
95. H. Chen, C. Yang, H. Ren, W. Zhang, X. Cui, Q. Tang, Water-Soluble Azobenzene-Based Solar Thermal Fuels with Improved Long-Term Energy Storage and Energy Density. *ACS Appl. Mater. Interfaces* **16**, 66837–66845 (2024). doi:10.1021/acsami.3c12264 Medline
96. R. J. Corruccini, E. C. Gilbert, The Heat of Combustion of *cis*- and *trans*-Azobenzene. *J. Am. Chem. Soc.* **61**, 2925–2927 (1939). doi:10.1021/ja01265a100
97. A. Gonzalez, M. Odaybat, M. Le, J. L. Greenfield, A. J. P. White, X. Li, M. J. Fuchter, G. G. D. Han, Photocontrolled Energy Storage in Azobispyrazoles with Exceptionally Large Light Penetration Depths. *J. Am. Chem. Soc.* **144**, 19430–19436 (2022). doi:10.1021/jacs.2c07537 Medline
98. G. D. Han, S. S. Park, Y. Liu, D. Zhitomirsky, E. Cho, M. Dincă, J. C. Grossman, Photon energy storage materials with high energy densities based on diacetylene–azobenzene derivatives. *J. Mater. Chem. A* **4**, 16157–16165 (2016). doi:10.1039/C6TA07086H
99. M. A. Morikawa, Y. Yamanaka, J. K. Ho Hui, N. Kimizuka, Photoliquefaction and

phase transition of *m*-bisazobenzenes give molecular solar thermal fuels with a high energy density. *RSC Adv.* **13**, 24031–24037 (2023). doi:10.1039/D3RA04595A Medline

100. Q. Qiu, M. A. Gerkman, Y. Shi, G. G. D. Han, Design of phase-transition molecular solar thermal energy storage compounds: Compact molecules with high energy densities. *Chem. Commun.* **57**, 9458–9461 (2021). doi:10.1039/D1CC03742K Medline
101. D. Schatz, C. Averdunk, R. Fritzius, H. A. Wegner, An Azobenzene-Based Liquid Molecular Solar Thermal (MOST) Storage System-Energy Carrier and Solvent. *Small* **21**, e2502938 (2025). doi:10.1002/smll.202502938 Medline
102. S. Sun, S. Liang, W.-C. Xu, M. Wang, J. Gao, Q. Zhang, S. Wu, Photoswitches with different numbers of azo chromophores for molecular solar thermal storage. *Soft Matter* **18**, 8840–8849 (2022). doi:10.1039/D2SM01073A Medline
103. W. Yang, Y. Feng, Q. Si, Q. Yan, P. Long, L. Dong, L. Fu, W. Feng, Efficient cycling utilization of solar-thermal energy for thermochromic displays with controllable heat output. *J. Mater. Chem. A* **7**, 97–106 (2019). doi:10.1039/C8TA05333B
104. N. Baggi, L. M. Muhammad, Z. Liasi, J. L. Elholm, P. Baronas, E. Molins, K. V. Mikkelsen, K. Moth-Poulsen, Exploring *ortho*-dianthrylbenzenes for molecular solar thermal energy storage. *J. Mater. Chem. A* **12**, 26457–26464 (2024). doi:10.1039/D4TA03879G Medline
105. T. Nishiuchi, S. Y. Uno, Y. Hirao, T. Kubo, Intramolecular Interaction, Photoisomerization, and Mechanical C–C Bond Dissociation of 1,2-Di(9-anthryl)benzene and Its Photoisomer: A Fundamental Moiety of Anthracene-Based π-Cluster Molecules. *J. Org. Chem.* **81**, 2106–2112 (2016). doi:10.1021/acs.joc.6b00134 Medline
106. H. P. Q. Nguyen, A. J. Maertens, B. A. Baker, N. M.-W. Wu, Z. Ye, Q. Zhou, Q. Qiu, N. Kaur, D. B. Berkinsky, K. E. Shulenberger, K. N. Houk, G. G. D. Han, Molecular Solar Thermal Energy Storage in Dewar Pyrimidone Beyond 1.6 MJ/kg, Dryad (2026). doi:10.5061/dryad.rxwdbrvqg
107. J. Browne, Options for Measuring Heat Capacity Using TA Instruments Discovery Series DSCs (TA Instruments, 2025); https://www.tainstruments.com/applications-notes/options-for-measuring-heat-capacity-using-ta-instruments-discovery-series-dscs-ta489/.
108. D. A. Ditmars, S. Ishihara, S. S. Chang, G. Bernstein, E. D. West, Enthalpy and Heat-Capacity Standard Reference Material: Synthetic Sapphire (α-Al_2O_3) from 10 to 2250 K. *J. Res. Natl. Bur. Stand.* **87**, 159–163 (1982). doi:10.6028/jres.087.012
109. C. Würth, M. Grabolle, J. Pauli, M. Spieles, U. Resch-Genger, Comparison of methods and achievable uncertainties for the relative and absolute measurement of photoluminescence quantum yields. *Anal. Chem.* **83**, 3431–3439 (2011). doi:10.1021/ac2000303 Medline
110. K.-L. Wong, J.-C. G. Bünzli, P. A. Tanner, Quantum yield and brightness. *J. Lumin.* **224**, 117256 (2020). doi:10.1016/j.jlumin.2020.117256
111. S. Babiak, A. C. Testa, Solvent effects on the fluorescence lifetime of 2-aminopyridine. *J. Phys. Chem.* **78**, 201–202 (1974). doi:10.1021/j100595a024
112. S. Babiak, A. C. Testa, Fluorescence lifetime study of aminopyridines. *J. Phys. Chem.* **80**, 1882–1885 (1976). doi:10.1021/j100558a015
113. M. J. Frisch, G. W. Trucks, H. B. Schlegel, G. E. Scuseria, M. A. Robb, J. R. Cheeseman, G. Scalmani, V. Barone, G. A. Petersson, H. Nakatsuji, X. Li, M. Caricato, A. V. Marenich, J. Bloino, B. G. Janesko, R. Gomperts, B. Mennucci, H. P. Hratchian, J. V. Ortiz, A. F. Izmaylov, J. L. Sonnenberg, D. Williams-Young, F. Ding, F. Lipparini, F. Egidi, J. Goings, B. Peng, A. Petrone, T. Henderson, D. Ranasinghe, V. G. Zakrzewski, J. Gao, N. Rega, G. Zheng, W. Liang, M. Hada, M. Ehara, K. Toyota, R. Fukuda, J. Hasegawa, M. Ishida, T. Nakajima, Y. Honda, O. Kitao, H. Nakai, T. Vreven, K. Throssell, J. A. Montgomery Jr., J. E. Peralta, F. Ogliaro, M. J. Bearpark, J. J. Heyd, E. N. Brothers, K. N. Kudin, V. N. Staroverov, T. A. Keith, R. Kobayashi, J. Normand, K. Raghavachari, A. P. Rendell, J. C. Burant, S. S. Iyengar, J. Tomasi, M. Cossi, J. M. Millam, M. Klene, C. Adamo, R. Cammi, J. W. Ochterski, R. L. Martin, K. Morokuma, O. Farkas, J. B. Foresman, D. J. Fox, Gaussian 16, Revision A.03 (Gaussian, Inc., 2016).
114. W. Kohn, L. J. Sham, Self-Consistent Equations Including Exchange and Correlation Effects. *Phys. Rev.* **140**, A1133–A1138 (1965). doi:10.1103/PhysRev.140.A1133
115. J.-D. Chai, M. Head-Gordon, Long-range corrected hybrid density functionals with damped atom-atom dispersion corrections. *Phys. Chem. Chem. Phys.* **10**, 6615–6620 (2008). doi:10.1039/b810189b Medline
116. S. Grimme, Semiempirical GGA-type density functional constructed with a long-range dispersion correction. *J. Comput. Chem.* **27**, 1787–1799 (2006). doi:10.1002/jcc.20495 Medline
117. F. Weigend, R. Ahlrichs, Balanced basis sets of split valence, triple zeta valence and quadruple zeta valence quality for H to Rn: Design and assessment of accuracy. *Phys. Chem. Chem. Phys.* **7**, 3297–3305 (2005). doi:10.1039/b508541a Medline
118. A. Schäfer, C. Huber, R. Ahlrichs, Fully optimized contracted Gaussian basis sets of triple zeta valence quality for atoms Li to Kr. *J. Chem. Phys.* **100**, 5829–5835 (1994). doi:10.1063/1.467146
119. F. Weigend, Accurate Coulomb-fitting basis sets for H to Rn. *Phys. Chem. Chem. Phys.* **8**, 1057–1065 (2006). doi:10.1039/b515623h Medline
120. A. V. Marenich, C. J. Cramer, D. G. Truhlar, Universal solvation model based on solute electron density and on a continuum model of the solvent defined by the bulk dielectric constant and atomic surface tensions. *J. Phys. Chem. B* **113**, 6378–6396 (2009). doi:10.1021/jp810292n Medline
121. S. Grimme, Supramolecular binding thermodynamics by dispersion-corrected density functional theory. *Chemistry* **18**, 9955–9964 (2012). doi:10.1002/chem.201200497 Medline
122. C. Gonzalez, H. B. Schlegel, An improved algorithm for reaction path following. *J. Chem. Phys.* **90**, 2154–2161 (1989). doi:10.1063/1.456010
123. G. Luchini, J. V. Alegre-Requena, I. Funes-Ardoiz, R. S. Paton, GoodVibes: Automated thermochemistry for heterogeneous computational chemistry data. *F1000 Res.* **9**, 291 (2020). doi:10.12688/f1000research.22758.1
124. Y.-P. Li, J. Gomes, S. Mallikarjun Sharada, A. T. Bell, M. Head-Gordon, Improved Force-Field Parameters for QM/MM Simulations of the Energies of Adsorption for Molecules in Zeolites and a Free Rotor Correction to the Rigid Rotor Harmonic Oscillator Model for Adsorption Enthalpies. *J. Phys. Chem. C* **119**, 1840–1850 (2015). doi:10.1021/jp509921r
125. C. Y. Legault, CYLview20 (Université de Sherbrooke, 2020); http://www.cylview.org.
126. K. Andersson, P. Å. Malmqvist, B. O. Roos, Second-order perturbation theory with a complete active space self-consistent field reference function. *J. Chem. Phys.* **96**, 1218–1226 (1992). doi:10.1063/1.462209
127. T. Shiozaki, W. Győrffy, P. Celani, H.-J. Werner, Communication: Extended multi-state complete active space second-order perturbation theory: Energy and nuclear gradients. *J. Chem. Phys.* **135**, 081106 (2011). doi:10.1063/1.3633329 Medline
128. T. Shiozaki, BAGEL: Brilliantly Advanced General Electronic-structure Library. *WIREs Comput. Mol. Sci.* **8**, e1331 (2018). doi:10.1002/wcms.1331
129. B. G. Levine, J. D. Coe, T. J. Martínez, Optimizing conical intersections without derivative coupling vectors: Application to multistate multireference second-order perturbation theory (MS-CASPT2). *J. Phys. Chem. B* **112**, 405–413 (2008). doi:10.1021/jp0761618 Medline
130. C. Riplinger, F. Neese, An efficient and near linear scaling pair natural orbital based local coupled cluster method. *J. Chem. Phys.* **138**, 034106 (2013). doi:10.1063/1.4773581 Medline
131. C. Riplinger, B. Sandhoefer, A. Hansen, F. Neese, Natural triple excitations in local coupled cluster calculations with pair natural orbitals. *J. Chem. Phys.* **139**, 134101 (2013). doi:10.1063/1.4821834 Medline
132. M. Nooijen, R. J. Bartlett, A new method for excited states: Similarity transformed equation-of-motion coupled-cluster theory. *J. Chem. Phys.* **106**, 6441–6448 (1997). doi:10.1063/1.474000
133. A. Sirohiwal, R. Berraud-Pache, F. Neese, R. Izsák, D. A. Pantazis, Accurate Computation of the Absorption Spectrum of Chlorophyll *a* with Pair Natural Orbital Coupled Cluster Methods. *J. Phys. Chem. B* **124**, 8761–8771 (2020). doi:10.1021/acs.jpcb.0c05761 Medline
134. N. Mardirossian, M. Head-Gordon, ωB97M-V: A combinatorially optimized, range-separated hybrid, meta-GGA density functional with VV10 nonlocal correlation. *J. Chem. Phys.* **144**, 214110 (2016). doi:10.1063/1.4952647 Medline
135. S. Grimme, J. Antony, S. Ehrlich, H. Krieg, A consistent and accurate *ab initio* parametrization of density functional dispersion correction (DFT-D) for the 94 elements H-Pu. *J. Chem. Phys.* **132**, 154104 (2010). doi:10.1063/1.3382344 Medline

136. S. Grimme, S. Ehrlich, L. Goerigk, Effect of the damping function in dispersion corrected density functional theory. *J. Comput. Chem.* **32**, 1456–1465 (2011). doi:10.1002/jcc.21759 Medline
137. F. Neese, F. Wennmohs, U. Becker, C. Riplinger, The ORCA quantum chemistry program package. *J. Chem. Phys.* **152**, 224108 (2020). doi:10.1063/5.0004608 Medline
138. F. Neese, The ORCA program system. *WIREs Comput. Mol. Sci.* **2**, 73–78 (2012). doi:10.1002/wcms.81
139. B. de Souza, F. Neese, R. Izsák, On the theoretical prediction of fluorescence rates from first principles using the path integral approach. *J. Chem. Phys.* **148**, 034104 (2018). doi:10.1063/1.5010895 Medline
140. S. H. Lin, H. Eyring, Study of the Franck-Condon and Herzberg-Teller Approximations. *Proc. Natl. Acad. Sci. U.S.A.* **71**, 3802–3804 (1974). doi:10.1073/pnas.71.10.3802 Medline
141. D. J. Brown, R. V. Forster, Pyrimidine reactions. XIV. The butylaminolysis of substituted methoxy-and methylthio-pyrimidines. *Aust. J. Chem.* **19**, 2321–2330 (1966). doi:10.1071/CH9662321
142. D. B. Ramachary, R. Mondal, Direct organocatalytic hydroalkoxylation of α,β-unsaturated ketones. *Tetrahedron Lett.* **47**, 7689–7693 (2006). doi:10.1016/j.tetlet.2006.08.134
143. D. J. Brown, M. N. Paddon-Row, The Dimroth rearrangement. Part X. The exceptionally slow rearrangement of 1,2-dihydro-2-imino-1,4-dimethylpyrimidines. *J. Chem. Soc. C* **1967**, 1928–1933 (1967). doi:10.1039/j39670001928
144. W. J. Hale, The constitution of acetylacetone-urea. *J. Am. Chem. Soc.* **36**, 104–115 (1914). doi:10.1021/ja02178a011
145. X. Zhuoxue, H. Yan, N. Yin, Y. Kou, Y. Tian, Q. Shi, Heat Capacity Study and Thermal Property Determination of trans-Azobenzene. *Russ. J. Phys. Chem.* **99**, 148–158 (2025). doi:10.1134/S0036024424703175

ACKNOWLEDGMENTS

Funding: NSF CAREER award DMR-2142887 (GGDH); 2025 Marion Milligan Mason Award for Women in the Chemical Sciences (AAAS) (GGDH); Alfred P. Sloan Foundation FG-2022-18328 (GGDH); Camille and Henry Dreyfus Foundation TC-23-028 (GGDH); Brandeis MRSEC DMR-2011846 (GGDH); RCSA Collaborative Innovation Award SA-SM3-2024-057b (GGDH); National Science Foundation CHE-215372 (KNH); National Science Foundation Graduate Research Fellowship DGE-2034835 (AJM); Gordon and Betty Moore Foundation through Grant GBMF13626 to UCSB (GGDH). **Author contributions:** Conceptualization: GGDH, KNH, HPQN; Funding acquisition: GGDH, KNH, KES; Investigation: HPQN, AJM, BAB, NMWW, YZ, QZ, QQ, NK, DBB; Methodology: HPQN, AJM; Project administration: GGDH; Supervision: GGDH, KNH; Visualization: GGDH, HPQN; Writing – original draft: HPQN, BAB, NMWW; Writing – review & editing: GGDH, KNH, HPQN, BAB, AJM, QZ. **Competing interests:** Authors declare that they have no competing interests. **Data, code, and materials availability:** All data are available in the main text or the supplementary materials. Data underlying the plots have been deposited at Dryad (*106*). **License information:** Copyright © 2026 the authors, some rights reserved; exclusive licensee American Association for the Advancement of Science. No claim to original US government works. https://www.science.org/about/science-licenses-journal-article-reuse

SUPPLEMENTARY MATERIALS

science.org/doi/10.1126/science.aec6413
Materials and Methods
Supplementary Text
Figs. S1 to S56
Tables S1 to S7
References (*107–145*)
Movies S1 to S5

Submitted 30 September 2025; accepted 27 January 2026
Published online 12 February 2026
10.1126/science.aec6413

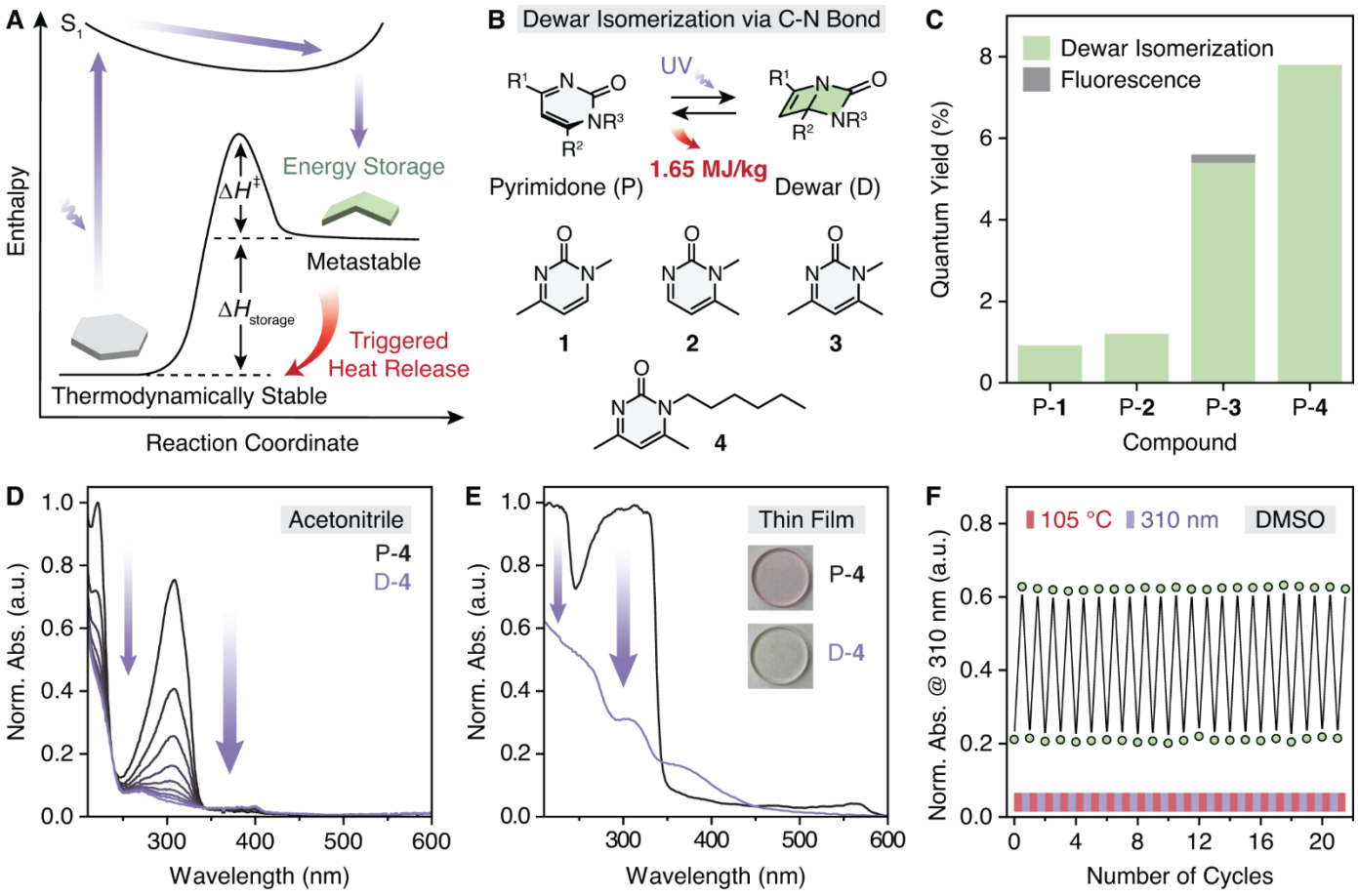


Fig. 1. Energy storage and release via reversible Dewar isomerization. (**A**) An energy diagram illustrating solar photon energy storage through Dewar isomerization and energy release by triggered electrocyclic ring-opening. (**B**) Reversible photo-induced Dewar isomerization of pyrimidone derivatives **1**–**4** with varied alkylation patterns. (**C**) Dewar isomerization quantum yield of P-**1** to P-**4** and fluorescence quantum yield of P-**3** in acetonitrile. (**D**) Normalized UV-Vis spectral changes upon the photoisomerization of P-**4** in acetonitrile obtained from irradiation at 310 nm. (**E**) Normalized thin-film UV-Vis absorption spectra of P-**4** and D-**4** obtained from irradiation at 310 nm. Insets display optical images of the thin film before and after irradiation corresponding to the UV-Vis spectra. (**F**) More than 20 cycles of reversible isomerization of D-**3** in dimethyl sulfoxide (DMSO) induced by thermal treatment at 105°C and subsequent irradiation at 310 nm.

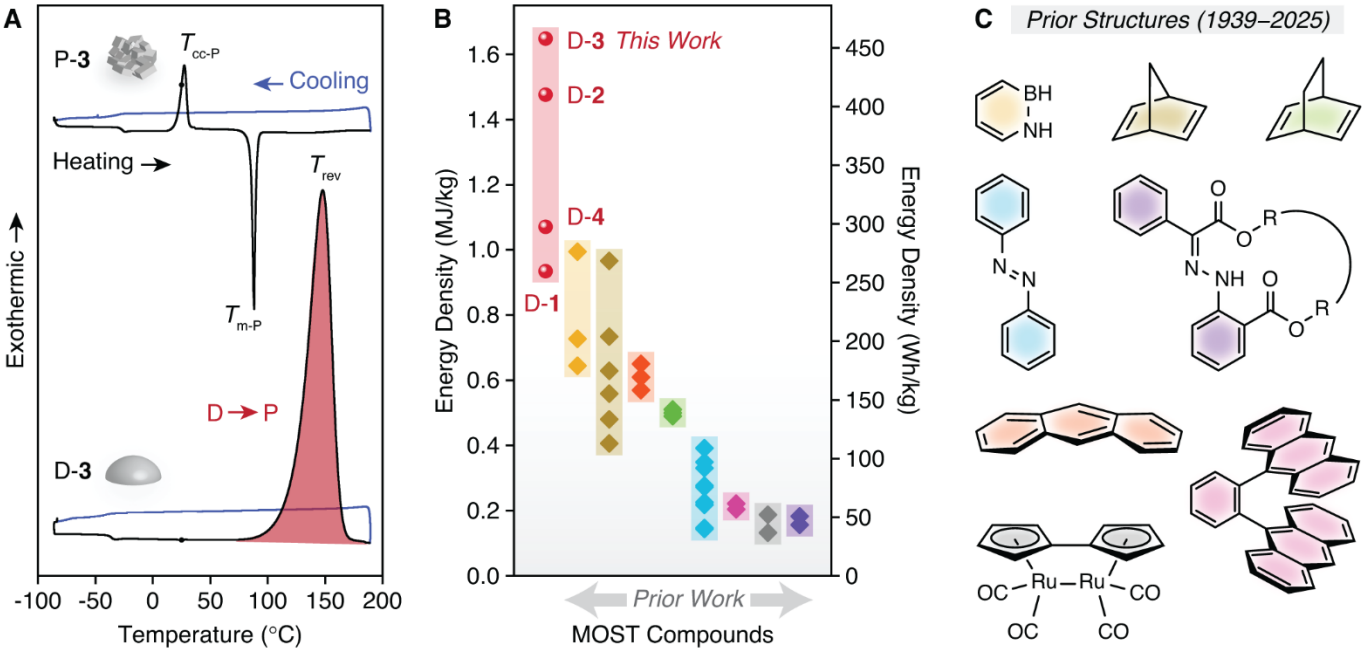


Fig. 2. Energy storage capacity of Dewar pyrimidones. (**A**) DSC thermograms of P-**3** and D-**3** measured during the first heating (black) and cooling (blue) cycle. Red highlighted area represents the exotherm of reversion ($\Delta H_{storage}$). T_{m-P}: melting point of pyrimidone; T_{cc-P}: cold crystallization point of pyrimidone; T_{rev}: peak thermal reversion temperature. The black dot on each plot marks the onset of data recording at the ambient temperature. (**B**) Gravimetric energy densities of Dewar isomers **1**–**4** compared to prior MOST photoswitches. (**C**) Chemical structures of prior MOST compounds, i.e., (left to right, top to bottom) azaborinines (*30*, *31*, *81*), norbornadienes (*23*–*28*), bicyclooctadienes (*29*), azo(hetero)arenes (*95*–*103*), hydrazones (*15*), curved anthracenes (*32*), *ortho*-dianthrylbenzenes (*104*, *105*), and fulvalene diruthenium (*19*, *20*).

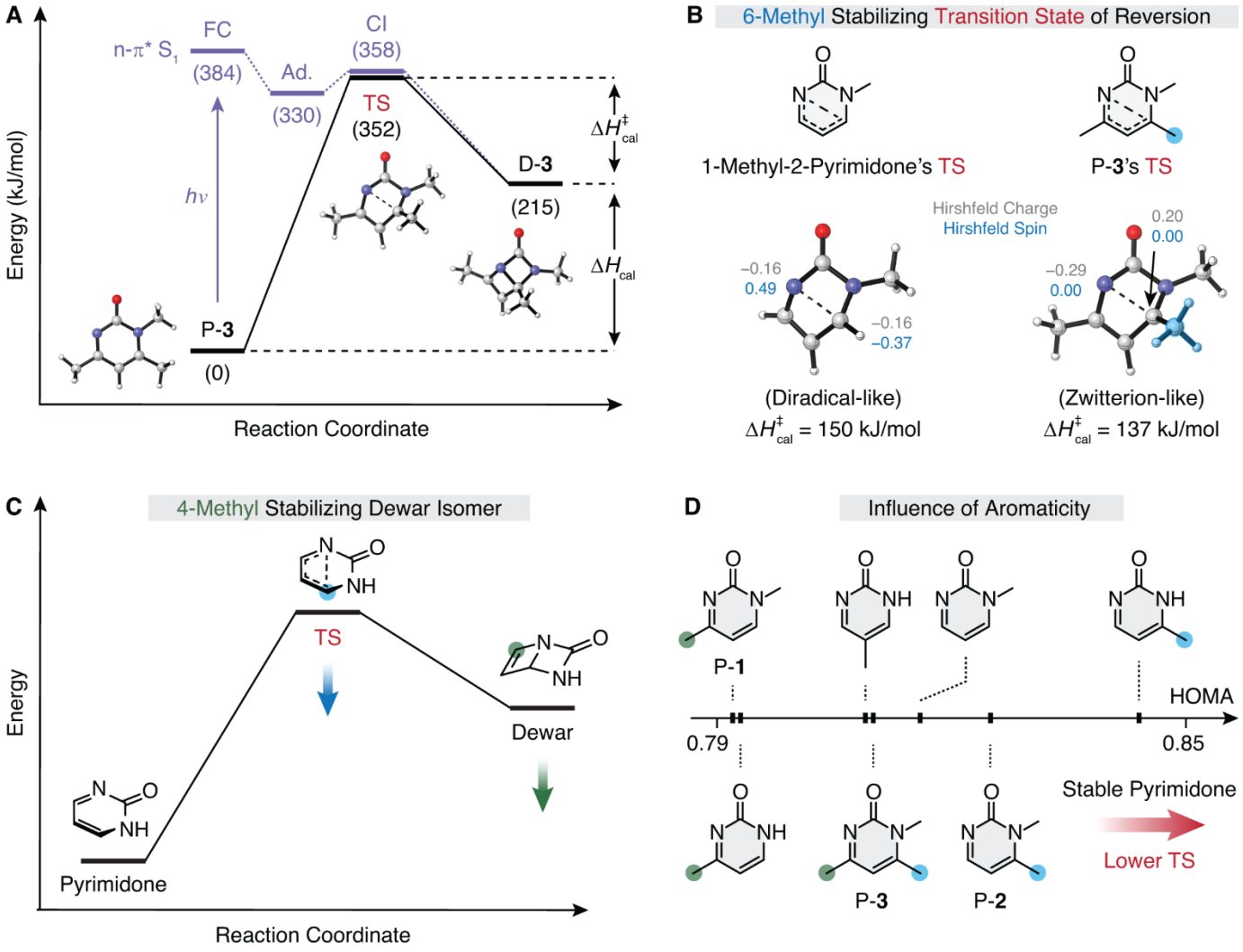


Fig. 3. DFT calculations of reversible Dewar isomerization process. (**A**) Photochemical Dewar isomerization mechanism of P-**3** (purple line) and thermal electrocyclic ring-opening mechanism of D-**3** (black line). (**B**) Hirshfeld charge and spin analysis of 1-methyl-2-pyrimidone and P-**3** in the transition state (TS) during the thermal reversion of their respective Dewar isomers. (**C**) Illustration of the stabilizing effect of a methyl substituent at the 4- and 6-positions on the Dewar 2-pyrimidone and the TS. (**D**) Correlation between Harmonic Oscillator Model of Aromaticity (HOMA) of pyrimidone derivatives and their TS energy. ΔH_{cal}: calculated energy storage density; $\Delta H^{\ddagger}_{cal}$: calculated enthalpy of activation. All enthalpies were calculated using (U)ωB97X-D/def2-TZVPP/PCM(DMF)//(U)ωB97X-D/def2-SVP/PCM(DMF) at 298.15 K and 1 atm. Excited state electronic energies were calculated at XMS-CASPT2(10e,8o)/def2-TZVPP//XMS-CASPT2(10e,8o)/def-2-SVP.

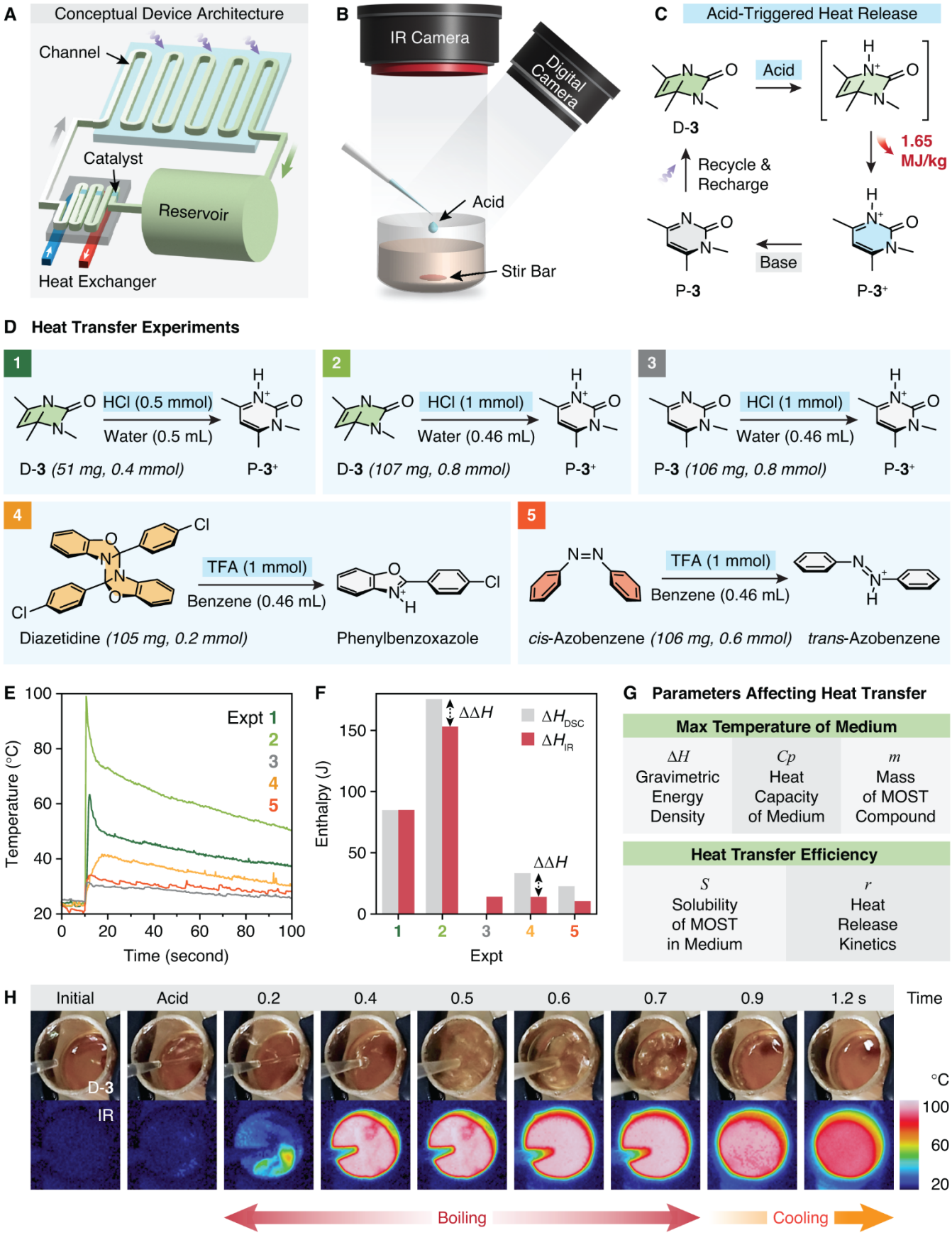

A
Conceptual Device Architecture
Channel
Catalyst
Reservoir
Heat Exchanger
B
IR Camera
Digital Camera
Acid
Stir Bar
C
Acid-Triggered Heat Release
D-3
Acid
1.65 MJ/kg
Recycle & Recharge
P-3
Base
P-3+
D Heat Transfer Experiments
1
HCl (0.5 mmol)
Water (0.5 mL)
D-3 (51 mg, 0.4 mmol)
P-3+
2
HCl (1 mmol)
Water (0.46 mL)
D-3 (107 mg, 0.8 mmol)
P-3+
3
HCl (1 mmol)
Water (0.46 mL)
P-3 (106 mg, 0.8 mmol)
P-3+
4
TFA (1 mmol)
Benzene (0.46 mL)
Diazetidine (105 mg, 0.2 mmol)
Phenylbenzoxazole
5
TFA (1 mmol)
Benzene (0.46 mL)
cis-Azobenzene (106 mg, 0.6 mmol)
trans-Azobenzene
E
Temperature (°C)
Time (second)
Expt 1
2
3
4
5
F
Enthalpy (J)
ΔΔH
ΔH_DSC
ΔH_IR
Expt
G Parameters Affecting Heat Transfer
Max Temperature of Medium
ΔH Gravimetric Energy Density
Cp Heat Capacity of Medium
m Mass of MOST Compound
Heat Transfer Efficiency
S Solubility of MOST in Medium
r Heat Release Kinetics
H
Initial
Acid
0.2
0.4
0.5
0.6
0.7
0.9
1.2 s
Time
D-3
IR
°C
100
60
20
Boiling
Cooling

Fig. 4. Macroscopic heat release and transfer. (**A**) Schematic representation of a conceptual MOST energy storage and release device operating in a closed-loop configuration (*85*, *86*). (**B**) Schematic of the experimental setup. A custom-made cylindrical glass vessel (15 mm in diameter) was used to hold the stirred sample solution. Temperature changes were recorded using a high-resolution infrared (IR) thermal imaging camera, and physical changes were captured with a digital camera positioned at a tilted angle. (**C**) Mechanism of acid-triggered thermal reversion of D-**3** to P-**3**. (**D**) Acid-triggered heat transfer experiments **1**–**5** conducted on different substrates, i.e., D-**3**, P-**3**, diazetidine, and *cis*-azobenzene. (**E**) Temperature profiles from experiments **1**–**5**. Temperatures were extracted from the hottest pixel (hot spot) on the surface of the solution. (**F**) DSC-measured heat release (ΔH_{DSC}) compared with IR-measured heat transfer (ΔH_{IR}) in experiments **1**–**5**. (**G**) Summary of key factors influencing heat transfer process. (**H**) Optical and IR images showing the physical and temperature change of D-**3** solution during acid-triggered heat release, demonstrating sufficient energy output to induce water boiling in experiment **2**.

Table 1. Thermal parameters for the retro-electrocyclization processes. T_{rev}: peak thermal reversion temperature; $\Delta H_{storage}$: energy storage density; $\Delta H^{\ddagger}$: enthalpy of activation; $t_{1/2}$: extrapolated half-life of Dewar isomer at 298 K; ΔH_{cal}: DFT calculated energy storage density; $\Delta H^{\ddagger}_{cal}$: DFT calculated enthalpy of activation.

D→P	T_{rev} (°C)	$\Delta H_{storage}$ (kJ mol^{-1})	$\Delta H_{storage}$ (MJ kg^{-1})	$\Delta H^{\ddagger}$ (kJ mol^{-1})	$t_{1/2}$ (days)	ΔH_{cal} (kJ mol^{-1})	$\Delta H^{\ddagger}_{cal}$ (kJ mol^{-1})
1	176.3 ± 3.3	132.9 ± 1.2*	1.070 ± 0.009*	N/A§	N/A§	225	156
2	134.6 ± 0.5	183.2 ± 3.7†	1.476 ± 0.030†	100.0 ± 3.1	80	222	135
3	148.7 ± 0.5	227.6 ± 1.4	1.648 ± 0.010	113.1 ± 2.3	481	215	137
4	159.8 ± 0.1	194.7 ± 0.6	0.935 ± 0.003	115.6 ± 0.9	1240	225	152

*Estimated $\Delta H_{storage}$ of 100% D-**1** derived from experimentally obtained $\Delta H_{storage}$ of 93:7 D-**1**/P-**1** mixture.
†Estimated $\Delta H_{storage}$ of 100% D-**2** derived from experimentally obtained $\Delta H_{storage}$ of 90:10 D-**2**/P-**2** mixture.
§D-**1** did not exhibit a clean thermal reversion to P-**1** and instead underwent decomposition below 80°C in DMSO, preventing the determination of reliable kinetic parameters.

Science
AAAS

Molecular solar thermal energy storage in Dewar pyrimidone beyond 1.6 MJ/kg

Han P. Q. Nguyen, Alexander J. Maertens, Benjamin A. Baker, Nathan M.-W. Wu, Zihao Ye, Qingyang Zhou, Qianfeng Qiu, Navneet Kaur, David B. Berkinsky, Katherine E. Shulenberger, K. N. Houk, and Grace G. D. Han

*Science***Ahead of Print** DOI: 10.1126/science.aec6413

View the article online
https://www.science.org/doi/10.1126/science.aec6413
Permissions
https://www.science.org/help/reprints-and-permissions

Use of this article is subject to the Terms of service

Science (ISSN 1095-9203) is published by the American Association for the Advancement of Science. 1200 New York Avenue NW, Washington, DC 20005. The title *Science* is a registered trademark of AAAS.

Copyright © 2026 The Authors, some rights reserved; exclusive licensee American Association for the Advancement of Science. No claim to original U.S. Government Works